

NIST Technical Note 1739

The Thermal Behavior of Structural Fire-Fighting Protective Ensemble Samples Modified with Phase Change Material and Exposed in Full-Scale Room Fires

Adam Barowy
Daniel Madrzykowski



FEMA

Sponsored in part by
Department of Homeland Security
Federal Emergency Management Agency
United States Fire Administration

NIST

National Institute of Standards and Technology
U.S. Department of Commerce

This page intentionally left blank

NIST Technical Note 1739

The Thermal Behavior of Structural Fire-Fighting Protective Ensemble Samples Modified with Phase Change Material and Exposed in Full-Scale Room Fires

Adam Barowy
Daniel Madrzykowski
Engineering Laboratory
National Institute of Standards and Technology

March 2012



FEMA

Department of Homeland Security
Janet Napolitano, *Secretary*
Federal Emergency Management Association
W. Craig Fugate, *Administrator*
United States Fire Administration
Ernest Mitchell Jr., *Administrator*



U.S. Department of Commerce
John E. Bryson, *Secretary*

National Institute of Standards and Technology
Patrick D. Gallagher, *Under Secretary of Commerce for*
Standards and Technology, and Director

Disclaimers

Use of Non-SI Units in a NIST Publication

It is NIST policy to use the International System of Units (metric units) in all its publications. In this report, however, information is presented in U.S. Customary Units (inch-pound), as this is the preferred system of units in the U.S. construction industry and fire service.

Certain commercial software, equipment, instruments, or materials may have been used in the preparation of information contributing to this report. Identification in this report is not intended to imply recommendation or endorsement by NIST, nor is it intended to imply that such software, equipment, instruments, or materials are necessarily the best available for the purpose.

Abstract

Phase change materials (PCM) have been suggested as a means to increase the thermal protective performance of structural fire fighting protective ensembles (FFPE) by taking advantage of the thermal energy required for to change phase. The National Institute of Standards and Technology (NIST) conducted full-scale compartment fire experiments to evaluate the thermal behavior of FFPE samples with PCM added, in a realistic fire fighting environment.

Two experiments were conducted, each in a single furnished compartment with one door and one window. FFPE assembly samples with an added mass of PCM equivalent in weight to 10 layers of batting and unmodified FFPE assembly samples were co-located in each compartment. Gas temperatures and heat fluxes were measured in multiple locations, as well as the inner and outer temperature of each FFPE assembly. This report contains analysis of the data collected, details of the fuel load, compartment construction and geometry, and the location and type of instrumentation. The results of these experiments demonstrate that the FFPE with PCM reduced the amount of thermal energy transferred through to the interior surface of the FFPE. However, the FFPE with PCM performed effectively the same as an unmodified FFPE once the compartment reached flashover conditions.

Key Words: fire fighter protective ensemble, heat stress, heat transfer, personal protective equipment, phase change materials, plate thermometer, reactive cooling systems, thermal environments, thermal injury, total heat flux, turnout gear

Table of Contents

NIST Technical Note XXXX	i
Abstract	i
Table of Contents	ii
List of Figures	iv
List of Tables	v
1. Introduction.....	1
2. Background.....	5
3. Technical Approach.....	9
3.1 Experimental Structure	9
3.2 Room Furnishings.....	11
3.3 Instrumentation	13
3.3.1 FFPE Sample Preparation	17
3.3.2 Plate Thermometer Heat Flux Calculation.....	20
3.4 Uncertainty Analysis.....	21
3.5 Experimental Procedure.....	22
4. Results.....	23
4.1 Experiment 1: Closed Door.....	23
4.1.1 Thermal Conditions inside the Compartment	23
4.1.2 Thermal Measurements from Sample Location	28
4.1.3 Heat Flux Measured with Plate Thermometer	31
4.2 Experiment 2: Open Door	32
4.2.1 Thermal Conditions inside the Compartment	32
4.2.2 Thermal Measurements from Sample Location.....	35
4.2.3 Heat Flux Measured with Plate Thermometer	39
5. Discussion.....	40
5.1 Impact of Phase Change Material	40
5.2 Impact of Ventilation	41
5.3 Plate Thermometer Heat Flux Measurement	44
6. Conclusions.....	44
6.1 Primary objectives: thermal energy transfer through and comparison of modified and unmodified FFPE samples	44
6.2 Secondary objectives: Impact of ventilation on compartment thermal conditions and exploratory use of plate thermometer.....	45
7. Future Work.....	45
8. Acknowledgements.....	46

9. References.....	46
Appendix A: Plate Thermometer Temperature Measurements	49
Appendix B: Bi-Directional Probe Pressure and Temperature Measurements	50

List of Figures

Figure 1: Time-Temperature Relationship for Burns [10].....	1
Figure 2: Assembly of 4 different layers making up FFPE, from outside-in (Batting and interior liner sewn together. PCM between batting/layers.)	6
Figure 3: Assembly of 4 different layers making up FFPE, from inside-out (Batting and interior liner sewn together. PCM between batting/layers.)	6
Figure 4: Phase change diagram	7
Figure 5: Photo showing a small sample of the phase change material.....	8
Figure 6: Exterior of the structure used for conducting the experiments.....	9
Figure 7: Dimensioned floor plan of the compartments used in the experiments.....	10
Figure 8: Positions of the contents (fuels) and ignition source placed into each compartment	11
Figure 9: Photographs of the contents placed into the compartment in experiment 1 (left) and experiment 2 (right)	11
Figure 10: Positioning of measurement instrumentation installed in compartments.....	13
Figure 11: Schematic of instrumentation array used for thermal measurement of the protective ensembles	15
Figure 12: Positioning of measurement instruments on wall behind protective ensemble samples	15
Figure 13: Positioning of bi-directional pressure probes and thermocouples measuring flow through the door and window. Measurements next to the instruments in the window indicate height above the sill. Measurements next to the instruments in the door indicate height above the threshold.....	16
Figure 14: Photograph showing the unmodified protective ensemble assembly (left) and the protective ensemble with phase change material added (right)	17
Figure 15: Placement of thermocouples in the protective ensemble assembly used to measure the thermal behavior of the phase change material	18
Figure 16: Photograph of the completed installation of the protective ensemble assembly with measurement instruments.....	19
Figure 17: Floor to ceiling temperatures measured by the thermocouple array in the center of the compartment in Experiment 1	23
Figure 18: Floor to ceiling temperatures measured by the thermocouple array in the corner in Experiment 1	24
Figure 19: Total heat flux measured by the heat flux gauge next to the PE samples and by the gauge in the center of the compartment on the floor in Experiment 1	25
Figure 20: Video frame capture of compartment conditions immediately prior to suppression, with locations of total HF gauges indicated	26
Figure 21: Velocity of gasses measured along the centerline of the front door in Experiment 1	27
Figure 22: Total heat flux compared with radiative heat flux measured in experiment 1	28
Figure 23: Comparison of the temperatures measured on the surface of the outer shell and the surface of the interior liner for the unmodified FFPE sample, Experiment 1.....	29
Figure 24: Temperatures measured on the surface of the outer shell and interior liner for the PE with PCM in Experiment 1	29
Figure 25: Total heat flux measured behind the unmodified FFPE and the FFPE with PCM in Experiment 1	30
Figure 26: View of the interior liner for the unmodified FFPE assembly (left) and the FFPE assembly with PCM added (right) after Experiment 1. Areas of discoloration highlighted.....	30
Figure 27: Comparison of the total heat flux measured by a S-B heat flux gauge and the total heat flux calculated from a plate thermocouple measurement in Experiment 1.	31
Figure 28: Floor to ceiling temperatures measured by the thermocouple array in the center of the compartment in Experiment 2.....	32
Figure 29: Floor to ceiling temperatures measured by the thermocouple array in the corner in Experiment 2	33

Figure 30: Total heat flux measured by the heat flux gauge next to the PE samples and by the gauge in the center of the compartment on the floor for Experiment 2.....	33
Figure 31: Velocity of gasses measured along the vertical centerline of the door in Experiment 2.....	34
Figure 32: Velocity of gasses measured along the vertical centerline of the window in Experiment 2.....	34
Figure 33: Comparison of the total heat flux measured by a S-B heat flux gauge and the radiative heat flux measurement in Experiment 2.....	35
Figure 34: Comparison of the temperature measure on the surface of the outer shell with the temperature measured on the surface of the interior liner of the unmodified FFPE in Experiment 2.....	36
Figure 35: Temperatures measured on the surface of the outer shell and interior liner for the PE with PCM in Experiment 2.....	36
Figure 36: Temperature measured behind the unmodified FFPE and the FFPE with PCM in Experiment 2.....	37
Figure 37: View of the interior liner for the FFPE with PCM (left) and the unmodified FFPE (right) after Experiment 2.....	38
Figure 38: Comparison of the total heat flux measured by a S-B heat flux gauge and the total heat flux calculated from a plate thermocouple measurement in Experiment 2.....	39
Figure 39: Thermal/mechanical damage to exterior of FFPE sample with PCM (left) and unmodified FFPE (right) after experiment two.....	41
Figure 40: Samples in oxygen-deficient hot layer, above flames, in Experiment 1.....	42
Figure 41: Samples in oxygen-deficient hot layer, above flames, in Experiment 2.....	42
Figure 42: Flames extend from the window and door due to oxygen-depleted (fuel-rich) conditions in the hot gas layer.....	43
Figure 43: Plate thermometer temperature measurement from between the FFPE samples, Experiment 149	
Figure 44: Plate thermometer measurement from between the FFPE samples, Experiment 2.....	49
Figure 45: Bi-Directional probe pressure measurements through doorway centerline, Experiment 1.....	50
Figure 46: Temperatures measured by thermocouples located in centerline of doorway, Experiment 1 ...	50
Figure 47: Bi-Directional probe pressure measurements through doorway centerline, Experiment 2.....	51
Figure 48: Temperatures measured by thermocouples located in centerline of doorway, Experiment 2 ...	51
Figure 49: Bi-Directional probe pressure measurements through window centerline, Experiment 2.....	52
Figure 50: Temperatures measured by thermocouples located in centerline of window, Experiment 2.....	52

List of Tables

Table 1: Layers of FFPE material making up test samples.....	5
Table 2: Details of the furnishings placed within the compartments.....	12
Table 3: Summary of measurement instrumentation.....	14

1. Introduction

In the period between 1977 and 2009, burns accounted for 19.5% of fire fighter fatalities that occurred while operating at a structure fires [1]. In general, the number of annual firefighter deaths that occurred while operating outside at structure fires decreased, while the number of annual fire fighter deaths that occur due to traumatic injuries (a statistic that includes burn injuries) that occurred during operations inside did not decrease [1]. The frequency of non-fatal burn injuries has decreased annually since 1981; however, there were still 1,940 reported burn injuries on the fireground in 2010 [2].

A structural fire fighting protective ensemble (FFPE) is designed to provide the user with protection from the high temperature and heat flux environments present during structural fire fighting. The National Fire Protection Association (NFPA) maintains a standard for structural FFPE as well as other types of protective ensembles. Other protective ensembles are designed for proximity fire fighting (NFPA 1971 [3]), wildland fire fighting (NFPA 1977 [4]), liquid (NFPA 1992 [5]) and vapor (NFPA 1991 [6]) hazardous materials, and chemical, biological, and radiological particulates (NFPA 1994 [7]).

Burn injuries can occur from exposure to the thermal energy produced by a fire through radiation from the flames, radiation and convection from hot combustion gases, conduction from contact with hot surfaces or any combination of these means. Fire fighters are most at risk from burn injuries when their protective garments become thermally loaded and come in contact with the surface of their skin. This is likely to occur when movement constricts FFPE, or when contact with an exterior surface compresses the FFPE [8].

The burning of human skin is a complex process of non-steady heat transfer. The rate of skin heating depends upon the temperature and heating capacity of the source, the heat capacity and thermal conductivity of the skin layers, blood flow (which may be reduced if the skin is compressed [9]), the thickness of the skin (varies by body location), and the change in thermal properties with respect to skin depth [10, 11]. In other words, burn injuries depend on the rate of thermal energy transfer to human tissue. This is depicted by Figure 1 from the American Society for Testing and Materials (ASTM) standard on contact burn injuries, ASTM C 1055 [10].

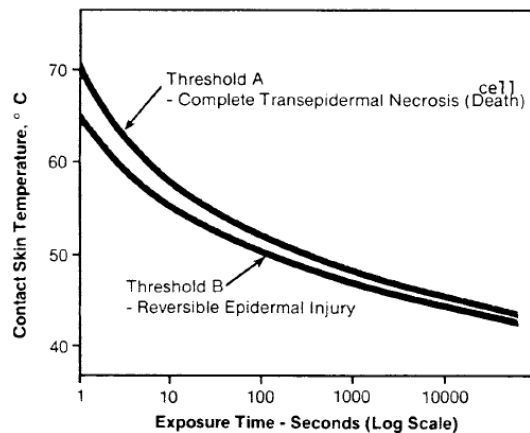


Figure 1: Time-Temperature Relationship for Burns [10]

In 1947, Moritz and Henriques conducted a series of burn injury experiments where both human and pig skin was exposed to a constant temperature and constant flow stream of hot water. They estimated that as the basal skin layer temperature increases above 44 °C (111 °F), the time to damage is shortened by approximately 50 % for each 1 °C rise in temperature, up to about 51 °C (124 °F) [12]. Starting in 1959 Stoll and Chianta performed tests on human, pig and rat skin with radiant heating apparatus [13, 14]. They found the same lower temperature bound (44 °C (111 °F)) for dermal necrosis as Moritz and Henriques, and that skin is almost instantaneously destroyed at 72 °C (162 °F) [15]. At temperatures above 70°C, the rate of injury from contact with a high heat capacity surface exceeds the body reaction time (less than 1 s to have completed epidermis cell death) such that the blood vessel location or flow has little effect on the level of burn¹ [12].

In 1991, Suzuki *et al.* studied longer term exposures of skin tissue to elevated temperatures. Starting in 1959, Stoll and Chianta performed tests on human, pig and rat skin with radiant heating apparatus [13, 14]. They found the same lower temperature bound (44 °C or 111 °F) for dermal necrosis as Moritz and Henriques, and that skin is almost instantaneously destroyed at 72 °C (162 °F) [15]. In 1991, Suzuki *et al.* discovered that deep dermal burns can occur at temperatures as low as 41.9 °C (107 °F) when exposed for several hours. Therefore, the amount of damage done to the skin is a function of both the temperature that the skin is exposed to, as well as the duration of thermal exposure. Based on Suzuki's research, thermal hazards begin to exist at approximately 41.9 °C (107 °F) [9].

The interior surface temperature of FFPE can easily exceed 41.9 °C (107 °F) while users operate in a fire fighting environment. The current edition of NFPA 1971 requires that structural FFPE materials withstand convective oven temperatures of 260 °C (500 °F) for at least five minutes [3]. Thus, FFPE may become thermally loaded without indication of degradation, and when compressed, cause thermal injury to the user.

Improvement of the protective performance of FFPE was identified as a high priority research issue in the National Fire Service Research Agenda [16], the NFPA Fire Service Protective Equipment Workshop [17] and the Innovative Fire Protection Workshop [18]. During the Innovative Fire Protection Workshop, passive cooling systems were suggested as a means to increase the thermal protective performance of FFPE. The proposed function of a passive cooling system would be to respond to short duration high thermal load, as in the case of flashover conditions or compressed gear. A passive system could use a chemical reaction or physical phase change to absorb heat energy in order to provide additional protection against burns. The system would ideally self-activate given a thermal energy criterion.

McCarthy conducted a series of bench-scale experiments to examine the feasibility of increasing the thermal protective performance of FFPE with the addition of a layer of phase change materials (PCM) between the interior liner and batting layers [19] (FFPE layers are described in Section 2). The experiments examined five different commercially available PCM that spanned a range of melting (phase change) temperatures from approximately 34 °C (93 °F) to 106 °C (223 °F). The tests were conducted under controlled laboratory conditions, at ambient room temperature, using a gas-fired radiant panel apparatus that conforms to the specifications in ASTM E162, Standard Test Method for Surface Flammability of Materials Using a Radiant Heat Energy Source [20]. The sample materials were radiatively exposed to heat fluxes of approximately 2.5 kW/m², 10 kW/m², and 20 kW/m².

¹ For perspective, previous experiments have shown the pain reaction to prolonged hyperthermia exposure first occurs as a stinging sensation typically between 47.5° and 48.5°C, but depends on the individual exposed [12].

Overall, lower temperatures were measured for the specimens with PCMs than those without. The temperature differences were largely due to the additional thermal mass of the PCM, but close examination of the temperature measurements for the layers near the PCM demonstrated additional energy absorption due to the phase change of the PCM. Of the 5 PCM tested, McCarthy determined that the PCM (“PCM B”) most likely to provide a thermal energy absorption advantage to FFPE melted between 44 °C (111 °F) and 55 °C (131°F) [19].

In addition to the bench-scale experiments, McCarthy developed a mathematical model of one dimensional heat transfer through an FFPE assembly with PCM. Using the model, McCarthy estimated that the experimental PCM configuration provided a thermal protective performance equivalent to two layers of batting material. The model could potentially be used for further research to investigate different types, quantities, and locations of PCM and FFPE materials in an FFPE assembly.

In 2005, Rossi et al performed a series of experiments similar to McCarthy’s [21]. Rossi treated coated the interior liner of 3 and 4-layer FFPE samples with similar micro-encapsulated PCM integrated into foam. The melting temperature of the PCM was approximately 50 °C (122 °F) and the application of the PCM and foam layer added approximately 180g/cm² to the samples. The FFPE samples were heated using the radiant heating apparatus from ISO 6942 [22](similar to ASTM E162), and the flame exposure apparatus from ISO 9151 [23] (similar to the thermal protective performance apparatus specified in NFPA 1971). The location of the PCM layer was also varied by reversing the orientation of the interior liner. In the radiant exposure experiments, the samples were exposed to heat fluxes of (5, 10 and 40) kW/m². Rossi found that the PCM layer increased the thermal protection of the 3-layer FFPE samples by an average of 44.8% relative to the untreated samples, and the 4-layer samples by a relative average of 37.0%. In general, the PCM layer was more effective when oriented towards the user-side of the assembly because the reaction time needed for the PCM. It should be noted that because of the PCM reaction time, Rossi suggests that the threshold time to pain and burn injuries may be reached before the PCM changed phase with higher intensity heat fluxes.

To follow-up on the bench-scale experiments, NIST conducted two full-scale fire experiments in single room enclosures that exposed unmodified FFPE samples and FFPE samples with PCM added, to the thermal conditions of a realistic fire-fighting environment. In addition to radiative heat transfer, a key feature was that the compartment fires included convection heat transfer from hot combustion effluent to the FFPE samples. With the radiant panel apparatus, radiantly heated samples experience convective losses to the cooler ambient laboratory environment.

In each experiment, one unmodified FFPE sample and one FFPE sample with PCM B were exposed to compartment fire conditions. The samples with PCM used the same type and quantity per unit area of PCM as in the bench-scale experiments [19]. In the first experiment, the compartment was unventilated until a door was opened after 5 minutes. In the second experiment, the door was open for the duration of the experiment. Two primary objectives of the experiments were to:

- Compare the thermal behavior of an unmodified FFPE sample with a sample of FFPE with PCM
- Quantify the thermal energy transfer through unmodified FFPE samples with and without a layer of PCM added, exposed to a realistic interior fire fighting thermal environment.

Given the opportunity to perform the full-scale experiments, supplementary instrumentation was included, and data analysis was performed to pursue two secondary objectives to:

- Examine the impact of ventilation on thermal conditions inside the compartment
- Explore plate thermometers as a simple, economical means to expand upon heat flux measurement capabilities in field experiments

These experiments were conducted by NIST with support from the Department of Homeland Security (DHS), and in cooperation with the United States Fire Administration, (USFA), National Fire Academy (NFA), and the Bureau of Alcohol, Tobacco, Firearms and Explosives (ATF).

2. Background

Structural fire fighting protective ensembles consist of at least four layers of material: an outer shell, a moisture barrier, thermal insulating material or “batting”, and an interior liner [3]. Each layer is designed to perform a primary protective function, though all of the layers, and the air gaps between them, impede thermal energy transfer to the user. Several textile manufacturers (e.g., DuPont®, W.L. Gore) produce different FFPE fabrics (e.g., Nomex®, Gore-Tex®) for each FFPE layer. Each type of material is designed with targeted performance characteristics to meet the different requirements and preferences of customers, including cost. The trade names of the layers of material used in these experiments are documented in Table 1. The specific materials used in the trademarked fabrics are proprietary. The layers were selected to match the sample setup in the bench-scale experiments [19].

Table 1: Layers of FFPE material making up test samples

	FFPE Layer	Material	Reference
Therma I Liner	Interior Liner (Glide 2-Layer)	100 % Nomex® Twill with Nomex® filament	[24]
	Batting (Glide 2-Layer)	1 layer of 1.5 osy of Nomex® / Kevlar® E-89 Spunlace 1 layer of 2.3 osy of Nomex® / Kevlar® E-89 Spunlace	[24]
	Moisture Barrier (Crosstech 2-Layer)	CROSSTECH™ Membrane (ePTFE) Nomex® Pajama Check (substrate)	[25]
	Outer Shell (PBI Matrix)	60% Kevlar® / 40% PBI with 600 denier Kevlar® cables	[26]

The interior liner, which is next to the skin, is primarily intended to provide comfort for the user by wicking moisture and reducing the friction between the assembly and the user’s clothes. The batting layer provides the bulk of the thermal insulation in the assembly, and in this case is sewn to the interior material². Moisture barrier materials are designed as a one-way membrane that prevents moisture from penetrating and compromising the thermally insulative properties of the batting and interior liner layers. Breathability is a particularly important variable to consider in moisture barrier design, because it directly affects comfort, drying time, and physiological stress. Control of water vapor with the moisture barrier in FFPE directly affects the heat transfer properties of the assembly. The outer shell’s primary purpose is to provide thermal and mechanical protection for the underlying layers, in addition to flame resistance [27]. Figure 2 and Figure 3 show a deconstructed assembly of FFPE with each layer labeled.

² Some ensembles provide an additional removable insulating layer for winter weather for coats. A winter liner is not required by NFPA 1971 [3].

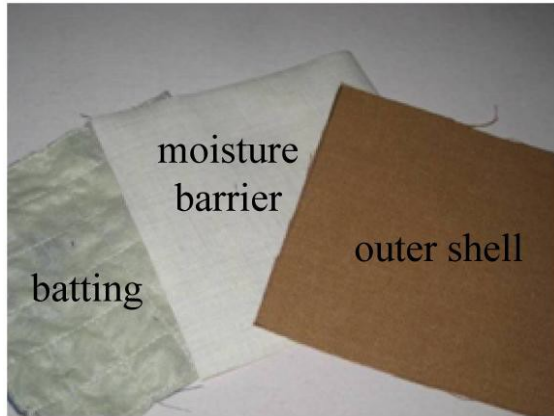


Figure 2: Assembly of 4 different layers making up FFPE, from outside-in (Batting and interior liner sewn together. PCM between batting/layers.)

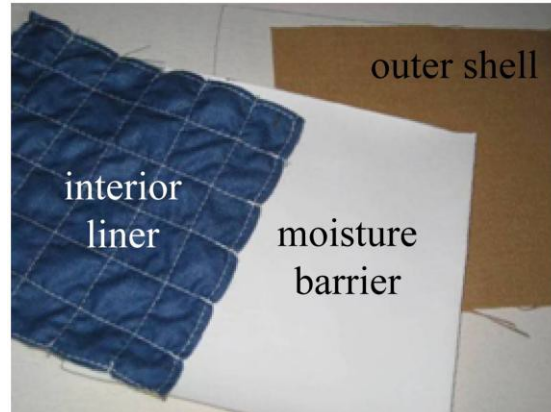


Figure 3: Assembly of 4 different layers making up FFPE, from inside-out (Batting and interior liner sewn together. PCM between batting/layers.)

Passive cooling systems are proposed to work by adding a layer of phase change materials between the batting and interior liner layers. As thermal energy is absorbed from the fire environment by the outer shell, the PCM layer would absorb energy and delay the energy transfer to the person using the FFPE. After enough energy is absorbed, the PCM layer would begin to change phase or melt. The change in phase is the physical mechanism proposed to provide additional thermal protection, without significantly decreasing the ease of movement when wearing FFPE. Additional thermal energy, beyond what is required to heat a material in one type of phase, is required to make a material change phase. Figure 4 shows a diagram that relates energy absorption and temperature to phase change.

As an example of phase change, consider water. When water is heated (absorbs thermal energy), it changes from a liquid to a vapor. The additional energy (latent heat of vaporization) required to change phase is what makes water effective at absorbing thermal energy. The high latent heat of vaporization of water is what makes it a particularly effective fire suppressant. When water vapor loses thermal energy it changes phase (condenses) back to a liquid. The additional energy to change phase from solid to liquid is the latent heat of fusion, and the additional energy to change phase from liquid to vapor is the latent heat of vaporization.

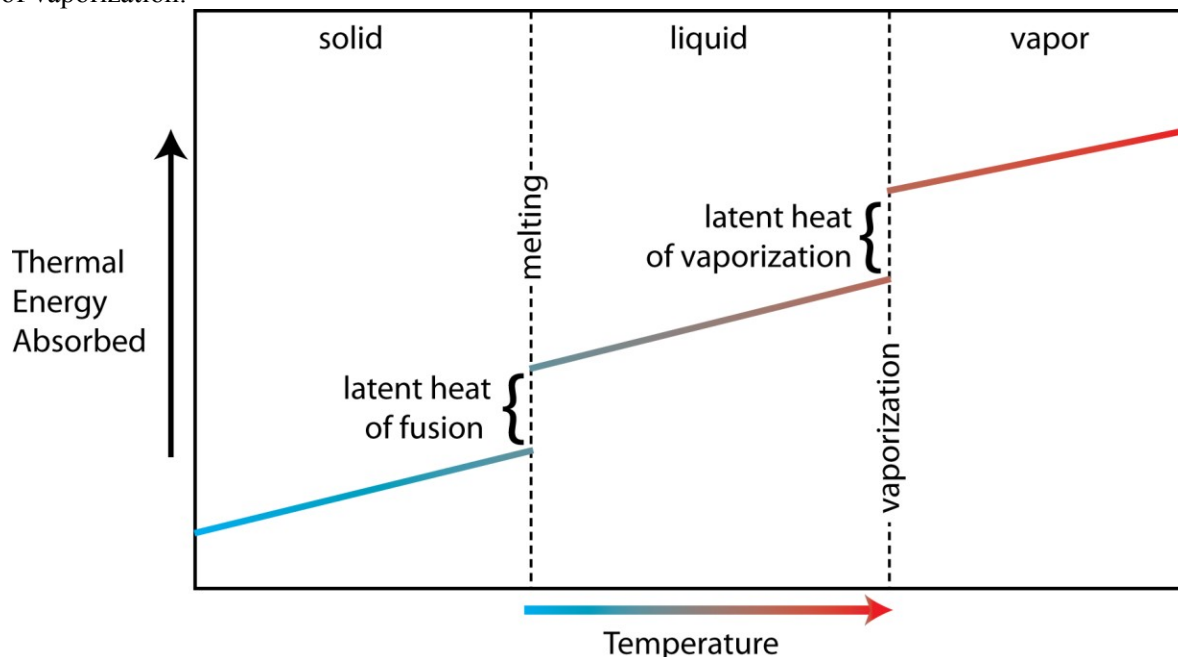


Figure 4: Phase change diagram

The PCM that may work best in FFPE, and that is considered in this study, would take advantage of the additional energy absorbed to overcome the latent heat of fusion. The PCM used in this study is designed as a “dry powder”, and is shown in Figure 5. The phase change material itself is paraffin based materials encapsulated in a secondary supporting structure made from a hydrophilic silica powder (SiO_2) [28]. The PCM inside melts within its support structure as it is heated. This is advantageous for preventing PCM leakage through layers of FFPE. The specific heat capacity of the PCM is 1.6 kJ/(kg·K) and the latent heat of fusion is 105 kJ/kg.



Figure 5: Photo showing a small sample of the phase change material

3. Technical Approach

Two experiments were conducted in a poured concrete compartment fire demonstration prop used for fire investigation. These experiments provide a representation of “real world” conditions, in terms of geometry, interior finish, materials and building elements, heat loss to the structure, ventilation, and volume. Each compartment was furnished with similar furniture. The fuel load was weighed and documented for each room.

Measurements were made to quantify and differentiate the level of thermal hazard and the rate of thermal hazard development in a furnished 2.65 m (8.7 ft) wide by 3.84 m (12.6 ft) long compartment with a 2.59 m (8.5 ft) high ceiling. In each compartment, temperature and heat flux measurements were made to provide information on the thermal conditions to which fire fighters operating in the compartment would be exposed. The experiments were also recorded with video cameras.

Additional temperature and heat flux measurements were made behind one sample of an unmodified protective ensemble assembly and one sample of the modified protective ensemble with a phase change material sewn between the interior liner and the batting layers. These measurements were made to compare the quantity and rate of thermal energy transfer through an unmodified protective ensemble with and without the addition of a phase change material.

The other key issue examined was the impact of a closed door (compartmentation) on fire spread and thermal conditions inside the room. Each experiment involved the ignition of a small fire in the corner of the seat cushion in the chair in the West corner of the room (Figure 7).

3.1 Experimental Structure

The structure used for the experiments was designed for compartment-fire demonstrations and training and had two cells. The structure is shown with instrumentation in Figure 6.

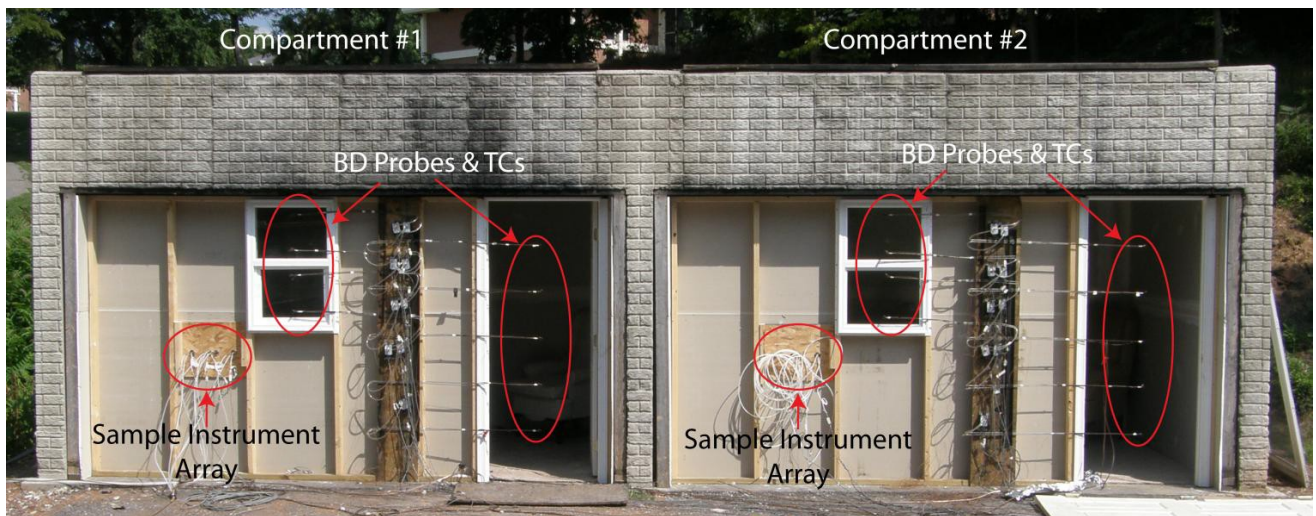


Figure 6: Exterior of the structure used for conducting the experiments

The permanent portion of the structure is constructed from poured concrete walls approximately 0.2 m (8 in) thick. Each cell has three permanent concrete walls. For these experiments, temporary walls were constructed inside the concrete walls, ceiling, and the open span of the compartments. This configuration simulated residential construction and protected the concrete from spalling damage. The studs in the wall construction were spaced 0.61 m (24 in) on-center. The gypsum used on the walls was 1.27 cm (0.50 in) thick. Seams between boards and fastener holes were sealed with spackling compound, but the board was not painted.

The final dimensions of the south compartment were 6.5 m (21.3 ft) wide by 3.84 m (12.6 ft) long with a 2.59 m (8.5 ft) high ceiling. Each compartment had a single doorway on the northeast side that measured 0.88 m (2.89 ft) wide by 2.02 m (6.63 ft) tall and a single double pane window on the east wall that measured 0.46 m (1.51 ft) wide by 0.76 m (2.5 ft) tall. The sill of the window was 1.18 m (3.87 ft) above the floor and the soffit was 0.63 m (2.1 ft) below the ceiling. The dimensions of the south (left in Figure 6) compartment are shown in Figure 7³.

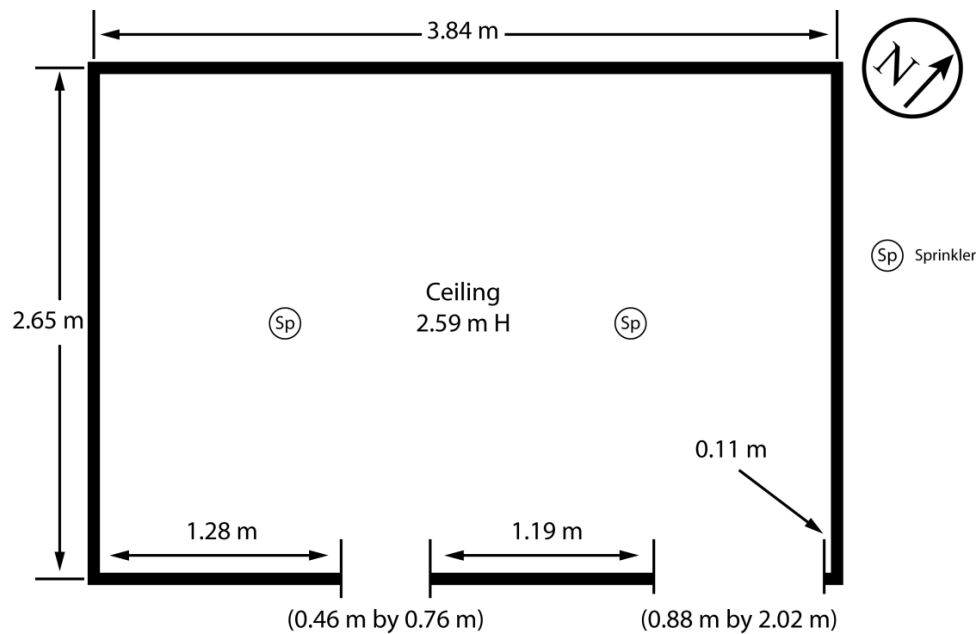


Figure 7: Dimensioned floor plan of the compartments used in the experiments

Oriented strand board (OSB) was laid over the concrete floor in each compartment, followed by polyester carpet. In each compartment, two ceiling mounted deluge sprinklers were connected to a manually activated water supply. The locations of the sprinklers are shown in Figure 7.

³ The corresponding dimensions of the north (right) compartment are 2.65 m (8.7 ft) wide by 3.86 m (12.6 ft) long with a 2.63 m (8.63 ft) ceiling. The windows and doors are the same dimensions.

3.2 Room Furnishings

The location and loading of furniture items was the same for both experiments. The primary sources of fuel were two upholstered chairs placed in opposite corners of the compartment, a small wooden television tray between the chairs, and the carpet on the floor. To a lesser extent, the paper face of the gypsum wallboard contributed to the fuel load. The positioning of the room contents is shown schematically in Figure 8. Figure 9 is a pair of photographs that show the actual contents in the rooms. Details that describe the dimensions, mass and materials used in each item placed in the compartment are given in Table 2.

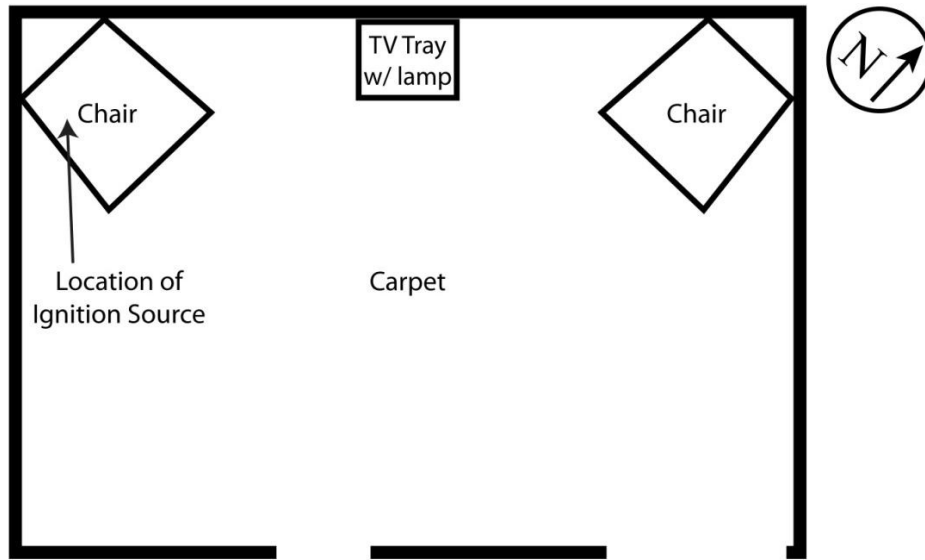


Figure 8: Positions of the contents (fuels) and ignition source placed into each compartment



Figure 9: Photographs of the contents placed into the compartment in experiment 1 (left) and experiment 2 (right)

Table 2: Details of the furnishings placed within the compartments

	Item	Material	Dimensions			Mass (kg)
			W (m)	L (m)	H (m)	
Room 1	Carpet	100% Polyester	3.84	2.71	-	20.2
	TV Tray	Wood	0.48	0.37	0.66 (top surface 0.02 thick)	3.0
	Green Chair	Wood frame, PU foam, Polyester batting	0.69	0.66	1.15 (arms 0.64, seat 0.48)	20.0
	White Chair	Wood frame, PU foam, Polyester batting	0.69	0.66	1.15 (arms 0.64, seat 0.48)	21.5
	Total =					64.7
Room 2	Carpet	100% Polyester	3.84	2.71	-	19.3
	TV Tray	Wood	0.48	0.37	0.66 (top surface 0.02 thick)	3.1
	Copper Chair	Wood frame, PU foam, Polyester batting	0.69	0.66	1.15 (arms 0.64, seat 0.48)	21.9
	Gold Chair	Wood frame, PU foam, Polyester batting	0.69	0.66	1.15 (arms 0.64, seat 0.48)	21.8
	Total =					66.1

3.3 Instrumentation

Instrumentation was selected and installed to measure the thermal environment inside the compartments and to quantify thermal energy transfer through the two assemblies of protective ensemble. Figure 10 shows the positioning of measurement instrumentation in a plan view of the compartments.

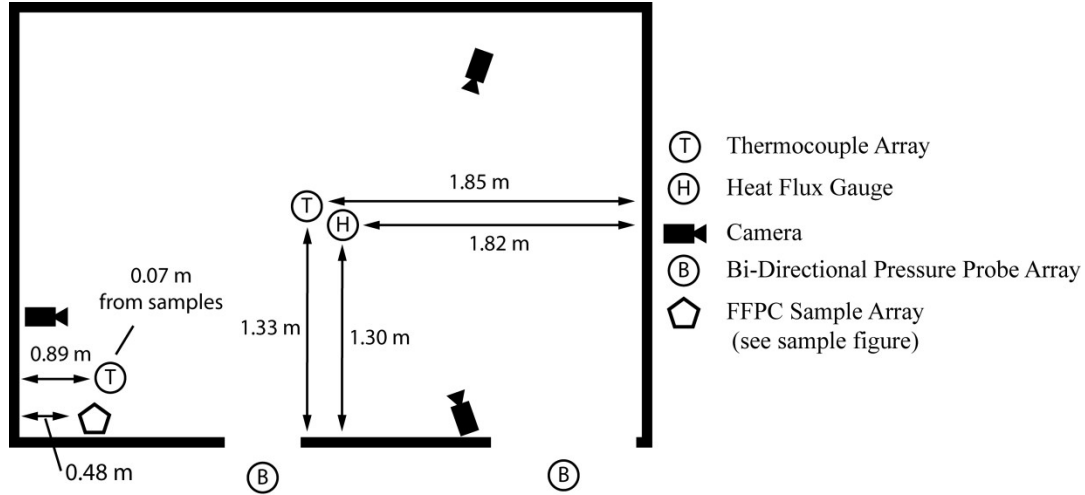


Figure 10: Positioning of measurement instrumentation installed in compartments

To measure compartment gas temperatures, vertical thermocouple arrays were placed in two positions. One array was positioned in the center of the compartment. The second array was positioned in the southwest corner of the compartment, centered between the PE samples. Each position had a vertical array of small diameter (AWG 30), bare bead, Type K thermocouples. In each array a thermocouple was located 25 mm, 0.305 m, 0.610 m, 0.910 m, 1.22 m, 1.52 m, 1.83 m, and 2.13m (1 in, 1 ft, 2 ft, 3ft, 4 ft, 5 ft, 6 ft, and 7 ft) below the ceiling.

Total heat flux was measured at two positions with Schmidt-Boelter (S-B) total heat flux gauges with a design heat flux measurement range up to 200 kW/m^2 ($17.6 \text{ Btu}/(\text{ft}^2 \cdot \text{s})$). One heat flux gauge was positioned on the floor, facing up, in the center of the compartment, next to the thermocouple array. The second heat flux gauge was positioned between the PE samples, facing the north wall, approximately 0.91 m (36 in) above the floor. Radiative heat flux was also measured with a S-B heat flux gauge modified with a quartz glass window (radiometer). The radiometer was co-located with the total heat flux gauge between the PE samples. The precise positioning of the heat flux gauges with respect to the PE samples is shown schematically in Figure 11

Table 3: Summary of measurement instrumentation

Instrument	Room Location	Orientation	Measurement
Thermocouple (Type K)	Behind unmod. FFPE	N/A	Interior Liner Temperature
Thermocouple (Type K)	Behind mod. FFPE	N/A	Interior Liner Temperature
Thermocouple (Type K)	Surface of unmod. FFPE	N/A	Outer Shell Temperature
Thermocouple (Type K)	Surface of mod. FFPE	N/A	Outer Shell Temperature
Thermocouple (Type K)	Between samples	N/A	Gas Temperature
Plate Thermometer	Behind unmod. FFPE	@ North wall	Total heat flux transferred through unmodified FFPE
Plate Thermometer	Behind mod. FFPE	@ North wall	Total heat flux transferred through modified FFPE
Plate Thermometer	Between samples	@ North wall	Total heat flux at wall surface
S-B heat flux gauge	Behind unmod. FFPE	@ North wall	Total heat flux transferred through unmodified FFPE
S-B heat flux gauge	Behind mod. FFPE	@ North wall	Total heat flux transferred through modified FFPE
S-B heat flux gauge	Between samples	@ North wall	Rad. heat flux at wall surface
Radiometer	Between samples	@ North wall	Total heat flux at wall surface
S-B heat flux gauge	Center/floor of compartment	@ Ceiling	Total heat flux at floor
Vertical Thermocouple Array (Type K)	Near samples, 0.07 m (3 in) from South wall	N/A	Floor to ceiling gas temperature profile
Vertical Thermocouple Array (Type K)	Center of compartment	N/A	Floor to ceiling gas temperature profile
Bi-directional probe array	Centerline of doorway	in/out of doorway	gas pressures/velocities through window
Bi-directional probe array	Centerline of window	in/out of window	gas pressures/velocities through window
Vertical Thermocouple Array (Type K)	Centerline of doorway	N/A	gas temperatures through door
Vertical Thermocouple Array (Type K)	Centerline of window	N/A	gas temperatures through window

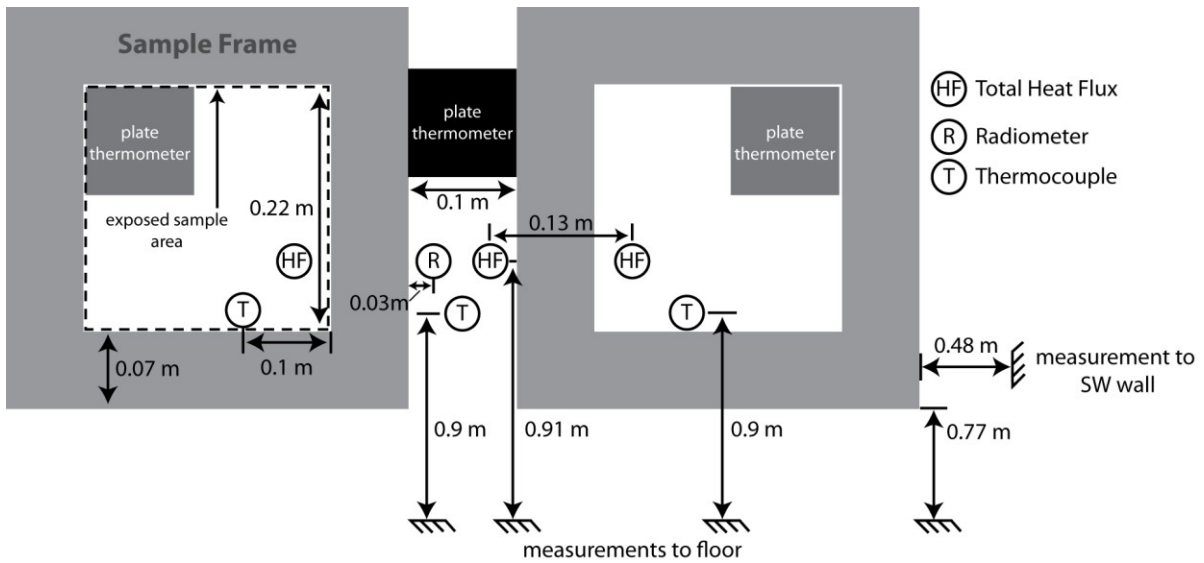


Figure 11: Schematic of instrumentation array used for thermal measurement of the protective ensembles

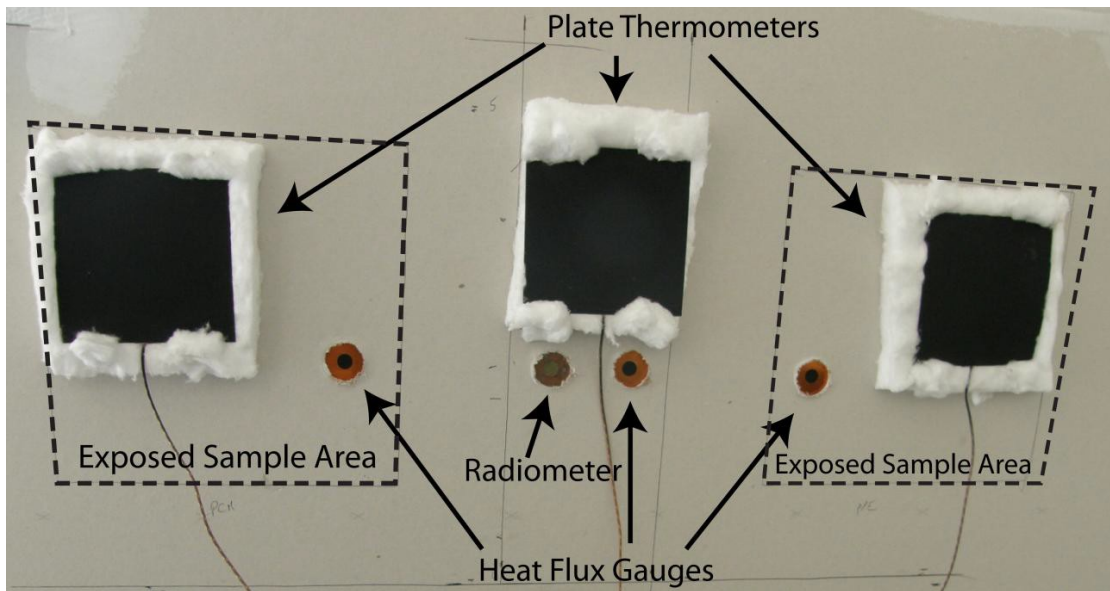


Figure 12: Positioning of measurement instruments on wall behind protective ensemble samples

Pressures were measured at 5 points along the centerline of the doorway 0.37 m, 0.70 m, 1.03 m, 1.36 m, and 1.69 m above the floor. Pressures were also measured at four points along the centerline of the window 0.05 m, 0.30 m, 0.44 m, and 0.75 m above the windowsill. Temperatures were measured at the ends of each bi-directional probe with 0.51 mm (0.02 in) nominal diameter bare bead Type K thermocouples for use in calculating the velocity of the gasses flowing in and out of the compartment. A schematic view of the placement of the probes is shown in Figure 13.

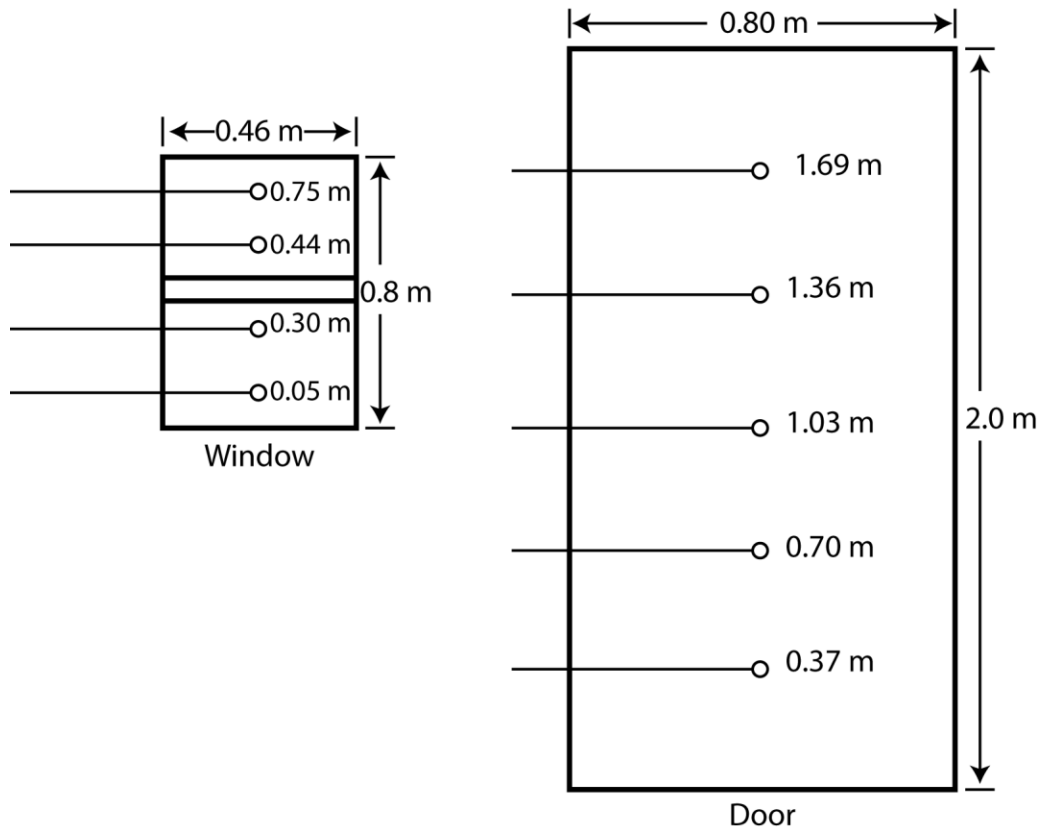


Figure 13: Positioning of bi-directional pressure probes and thermocouples measuring flow through the door and window. Measurements next to the instruments in the window indicate height above the sill. Measurements next to the instruments in the door indicate height above the threshold.

An additional total heat flux measurement was taken using a plate thermometer located between the PE samples, with bottom edge of the thermometer 0.94 m (37 in) above the floor. Each plate thermometer was constructed from a 24-gauge type K thermocouple welded to a steel plate sized approximately 0.1 m (4 in) by 0.1 m (4 in) by 1 mm (0.04 in) thick. The back face of each thermometer was insulated with a 152 mm (2 in) thick piece of high temperature spun fiber ceramic blanket, which also insulated the plates from the screws used to attach the instruments to the wall [29]. The front face of each plate thermometer was painted with high emissivity black paint ($\epsilon=0.95$) typically used on the surface of total heat flux gauges. The algorithm used to calculate total heat flux from the temperature measured by the plate thermometer is given in Section 3.3.2. A single type K thermocouple was placed between the heat flux gauges to measure the ambient gas temperature required for calculating total heat flux from the plate thermometer measurement. Measurements from the plate thermometers shown on the left and right in Figure 12, taken behind the FFPE samples, are not included in this report. Covering the plate thermometer with the FFPE samples changed the boundary conditions of the plate. Using the calculation method provided in Section 3.3.2 resulted in a poor comparison between the covered plate thermometer and the covered S-B heat flux gauge.

Eliminating the radiation and convection terms (leaving just the storage term) of the energy balance to account for the changed boundary conditions, did not improve the comparison for the changed heat transfer behavior as compared with an exposed plate thermometer.

3.3.1 FFPE Sample Preparation

One 0.51 mm (0.02 in) nominal diameter bare bead, Type K thermocouple was stitched to the outer shell of each FFPE sample assembly, exposed to the compartment environment. The thermocouple was positioned approximately 0.9 m (35 in) from the floor and 0.1 m from the inside edge of the mounting frame. A second thermocouple was stitched to the interior liner, representing a measurement “inside” the protective ensemble. Figure 14 is a photograph of the thermocouples stitched to the interior liner of both samples. The PCM was sewn into the samples by first unstitching the interior liner and batting layers. The PCM was weighed and distributed evenly across the batting layer. Finally, the interior liner and batting layer were stitched back together. The sample on the left in Figure 14 shows the original stitching from the manufacturer, and the completed stitching of the modified sample is shown on the right.

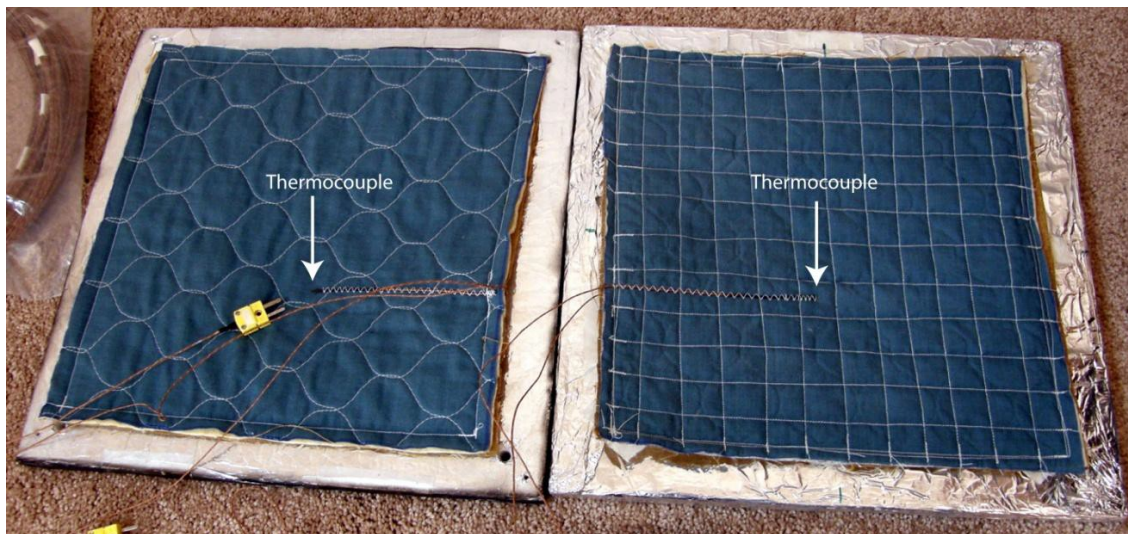


Figure 14: Photograph showing the unmodified protective ensemble assembly (left) and the protective ensemble with phase change material added (right)

Figure 15 shows an exploded assembly view of the FFPE samples with the thermocouples. Figure 15 also shows the stitching pattern used to contain the phase change material into “cells” between the interior liner and batting layers. The distribution of PCM within the samples was kept the same as the distribution used in McCarthy’s bench-scale experiments [19]. McCarthy used 15 g of PCM in a 152 mm by 152 mm sample, to represent the equivalent weight of approximately ten layers of batting material. The samples used in these experiments were sized approximately 305 mm by 305 mm, or 4 times larger than the bench-scale experiments. This was done to minimize the effects of the sample frame on the samples, and also to give an improved representation of the surface area of a fire fighter in FFPE. Approximately 60 g of PCM was sewn into the FFPE to have the same distribution of PCM.

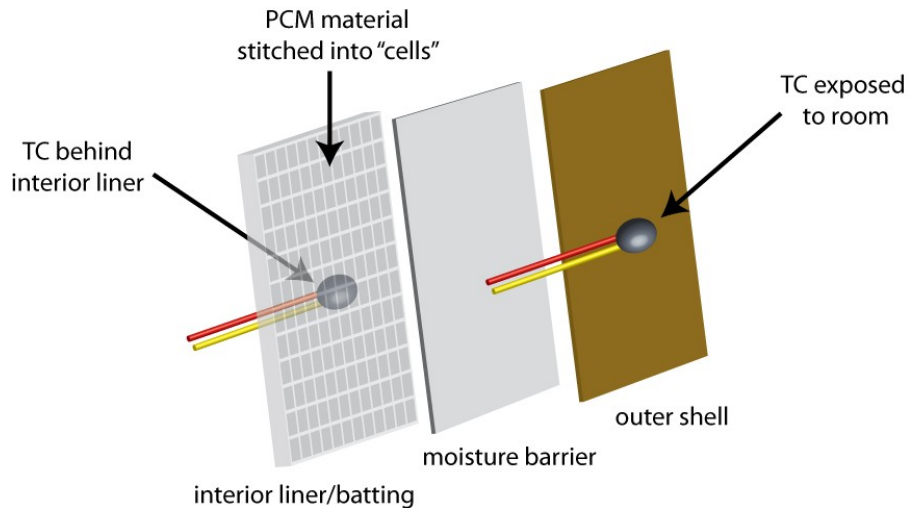


Figure 15: Placement of thermocouples in the protective ensemble assembly used to measure the thermal behavior of the phase change material

Each sample was mounted to the East compartment wall in a frame measuring approximately 0.36 m by 0.36 m (14 in by 14 in) made from 0.13 m (0.5 in) thick calcium silicate board. The hole cut into the center of the calcium silicate board was sized so that an area of FFPE sample measuring approximately 0.22 m by 0.22 m (8.5 in by 8.5 in) was exposed. The calcium silicate board was covered in aluminum foil to reduce the amount of thermal energy absorbed by the frames and transmitted into the samples. Figure 16 is a photograph that shows the final assembly of the FFPE samples and measurement instruments. There was no conditioning of the samples with regard to temperature or humidity prior to the experiments. The samples were initially stored in an office space, and installed just prior to the experiments

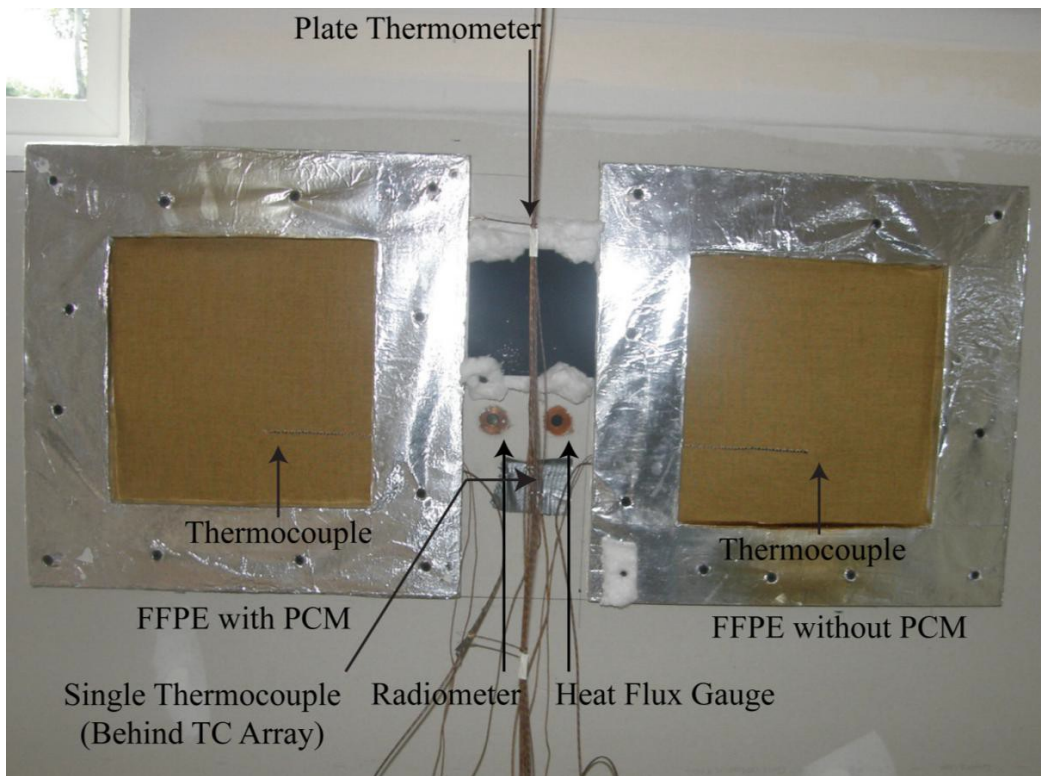


Figure 16: Photograph of the completed installation of the protective ensemble assembly with measurement instruments

The location of the samples was selected so that the samples would be in the least direct path of the inflow of oxygen from the door, in a “dead corner.” In other words, the samples were positioned in the region of the compartment that was expected to be the most oxygen deficient when the fire conditions were under-ventilated. This was intended to provide as uniform a total heat flux to as possible to both samples, as well as to prevent exposing the samples to direct flame contact. The high total heat flux that the samples would have been exposed to during direct flame contact would have rapidly damaged the samples and prevented the collection of useful data.

3.3.2 Plate Thermometer Heat Flux Calculation

Total heat flux was calculated from temperatures measured by the plate thermometer using the thermal energy balance developed by Ingason and Wickström [30], based on theory developed by Wickström [31]. Total heat flux is calculated as follows:

Eq. 1: Plate thermometer heat flux calculation from Wickström

$$q_{inc} = \frac{\varepsilon_{PT}\sigma T_{PT}^4 + h_{PT} + K_{cond} T_{PT} - T_{\infty} + \rho_{st}c_{st}\delta \frac{\Delta T_{PT}}{\Delta t}}{\varepsilon_{PT}}$$

Where:

q_{inc} = incident heat flux (W/m²)

ε_{PT} = emissivity of the thermometer surface (dimensionless) = 0.95⁴

σ = Stefan-Boltzmann constant (W/m² K⁴) = 5.67 E-10

T_{PT} = measured plate thermometer temperature (°K)

h_{PT} = convective heat transfer coefficient (W/m² K) = 10 W/m²K

K_{cond} = conduction correction factor (W/m² K) = 5 W/m²K

T_{∞} = measured temperature of gas surrounding plate thermometer (°K)

ρ_{st} = density of steel plate (kg/m³) = 8100 kg/m³

c_{st} = specific heat of steel plate (J/kg K) = 460 J/kg K

δ = thickness of steel plate (m) = 0.001 m

t = time (s)

The thermo-physical properties for steel, and heat transfer coefficients were taken from Ingason and Wickström's paper, as the plate thermometers were designed based on their specifications [30].

⁴ Paint manufactured by the Medtherm Corporation. Product literature is unavailable. The emissivity is listed on the spray can.

3.4 Uncertainty Analysis

There are different components of uncertainty in the length, temperature, heat flux, gas concentrations, mass and flow rate provided in this report. Uncertainties are grouped into two categories according to the method used to estimate them. Type A uncertainties are those that are evaluated by statistical methods and Type B are those that are evaluated by other means [32]. Type B analysis of systematic uncertainties involves estimating the upper (+ a) and lower (− a) limits for the quantity in question such that the probability that the value would be in the interval ($\pm a$) is very close to 100 %. For some of these components, such as the zero and calibration elements, uncertainties are derived from instrument specifications. Here uncertainty is reported as the expanded relative uncertainty with an expansion factor of two (i.e. 2σ).

Each length measurement was taken carefully. Length measurements such as the room dimensions, instrumentation array locations and furniture placement were made with steel tape measures with a resolution of ± 0.5 mm (0.02 in). However, conditions affecting the measurement, such as levelness or tautness of the device, yield an estimated uncertainty of ± 0.5 % for measurements in the 0.0 m (0 ft) to 3.0 m (9.8 ft) range. Some issues, such as “soft” edges on the upholstered furniture, or longer distances in excess of 3.0 m (9.8 ft) result in an estimated total expanded uncertainty of ± 1.0 %.

The standard uncertainty in temperature of the thermocouple wire itself is ± 2.2 °C at 277 °C and increases to ± 9.5 °C at 871 °C as determined by the wire manufacturer [33]. The variation of the temperature in the environment surrounding the thermocouple is known to be much greater than that of the wire uncertainty [34, 35]. Small diameter thermocouples were used to limit the impact of radiative heating and cooling. The estimated total expanded uncertainty for temperature in these experiments is ± 15 %.

Currently, there is little in the literature regarding the estimated uncertainty of the incident radiative flux calculated from plate thermometer measurements. Robbins provided an estimated uncertainty of $\pm 10\%$ for quasi-steady state measurements [36]. Further work outside of this study should be conducted to assess the influence of plate thermometer design features on measurement uncertainty (e.g., uniformity of insulation behind plate, method of connection of the thermocouple to the plate, emissivity of surface, etc.).

In this study, total heat flux measurements were made with water-cooled S-B gauges. The manufacturer reports a ± 3 % calibration expanded uncertainty for these devices [37]. Results from an international study on total heat flux gauge calibration and response demonstrated that the expanded uncertainty of a S-B gauge is typically $\pm 8\%$ [38].

Differential pressure reading uncertainty components were derived from pressure transducer instrument specifications and previous experience with pressure transducers. The transducers were factory calibrated and the zero and span of each was checked in the laboratory prior to the experiments yielding an accuracy of ± 1 % [39]. The total expanded uncertainty was estimated at 10 %.

Bi-directional probes and single thermocouples were used to measure the velocity. The bi-directional probes used similar pressure transducers as those used for the differential pressure measurements. Bare-bead Type K thermocouple are co-located with the probe. The estimated total expanded uncertainty for velocity in these experiments is ± 18 %.

The load cell used to weigh the fuels prior to the experiments had a range of 0 kg (0 lbs) to 200 kg (440 lbs) with a resolution of a 0.05 kg (0.11 lb) and a calibration uncertainty within 1% [40]. The expanded uncertainty is estimated to be $\pm 5\%$.

3.5 Experimental Procedure

Prior to ignition in each experiment, a computerized data acquisition system was started to collect the temperature, pressure, heat flux and plate thermometer data. Data were collected from each instrument every second. Video cameras recording the experiment were also started at this time. After at least 60 s of background data were collected, an electric match⁵ placed between the seat cushion and arm of the chair was used to ignite the upholstered chair in the corner farthest from the door.

The fire growth was observed via monitors connected to the video cameras. When the fire in the first compartment began to roll over and transition to flashover, the two deluge nozzles mounted near the ceiling were used to provide initial fire suppression. The second compartment was allowed to complete transition through flashover to a fully developed compartment fire. A team of fire fighters provided complete fire suppression in both experiments.

⁵ An electric match is a book of matches with a length of nickel-chromium resistance wire interwoven among the match heads. The wire heats up and ignites the matches when an electrical current is passed through the wire.

4. Results

The results of the experiments include experiment timelines based on observations, temperature and heat flux measurements, heat fluxes calculated from plate thermometer measurements, photographs and videos. An error bar that represents the total expanded uncertainty is included in each graph at the point of maximum value.

4.1 Experiment 1: Closed Door

The objective of this experiment was to measure the thermal conditions developed by a fire in a closed compartment, the change in conditions after the door is opened, and the subsequent thermal response of the modified and unmodified FFPE samples. Both the door and the window were initially closed when the fire was ignited. After approximately 280 s, the front door was opened. Flames extended across the compartment and impinged on the window and the interior upper and bottom panes cracked. However, the exterior panes held up and prevented additional ventilation. As the fire began transition to flashover, the fire was suppressed with the two deluge sprinklers installed in the compartment. The fire was then extinguished by fire fighters with a 4.4 cm (1 ¾ in) diameter hose line at approximately 530 s.

4.1.1 Thermal Conditions inside the Compartment

Figure 17 shows the temperature data from the thermocouple array in the center of the compartment. The temperature 25 mm (1 in) below the ceiling initially peaked at approximately 300 °C ± 45 °C (570 °F ± 85 °F), approximately 160 s after ignition.

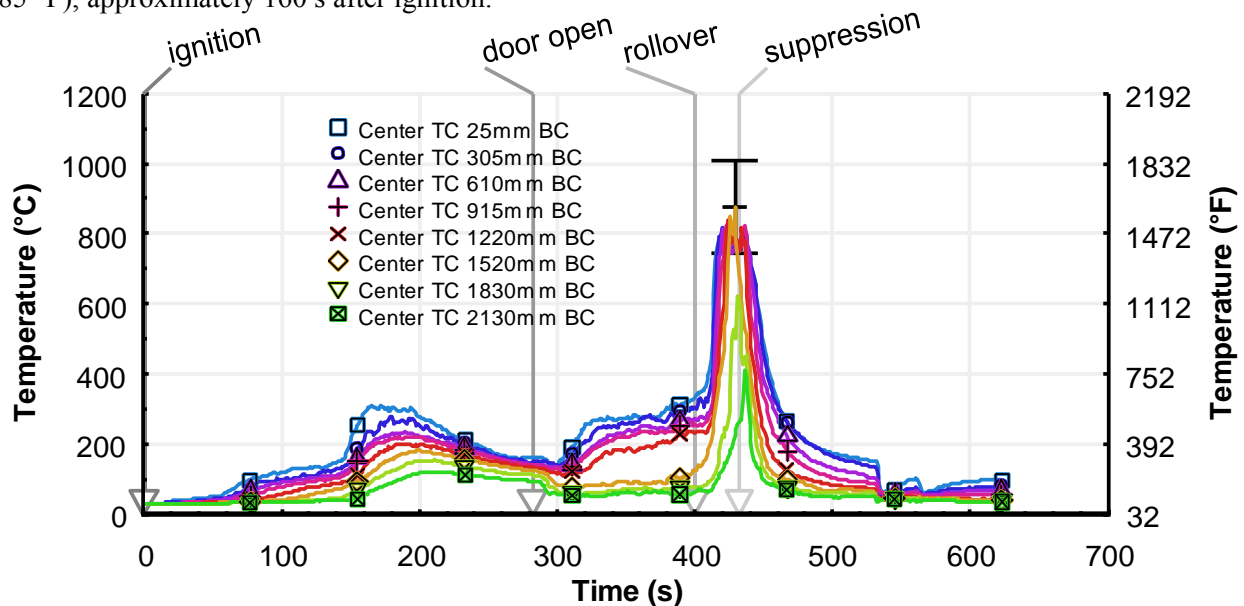


Figure 17: Floor to ceiling temperatures measured by the thermocouple array in the center of the compartment in Experiment 1

Prior to 160 s, heat and smoke from the chair formed a hot upper layer in the room, above a cool lower layer of ambient air. By approximately 160 s, the hot gas layer interface descended to roughly 48 cm (19 in), or the same height as the seat cushion in the burning chair. Within seconds, the hot gas layer interface descended further and the flames involving chair were completely obscured from video camera view by the smoke. Because the flames involving the chair were vitiated, flaming combustion was reduced, and the temperature gradient from floor to ceiling steadily decreased. As this occurred the hot

gas layer cooled, and the hot gas layer interface descended further. This caused the two-layer condition to transition into a relatively homogenous floor to ceiling smoke layer.

Approximately 280 s after ignition, the front door was opened. Fresh outside air flowed in through the bottom portion of the open door and hot gasses flowed out the top portion. Within 40 s of the door being opened, the two-layer condition returned. Measurements from the thermocouple array show a distinct hot gas layer and cooler lower layer. With the increase in ventilation, the fire involving the chair became gradually less vitiated and flaming combustion increased.

Temperatures in the hot gas layer increased steadily, while temperatures in the lower layer remained near ambient, until rollover⁶ occurred. After rollover occurred, the temperatures rapidly increased from floor to ceiling. A peak temperature of $900\text{ °C} \pm 135\text{ °C}$ ($1650\text{ °F} \pm 250\text{ °F}$), was recorded 25 mm (1 in) below the ceiling. After rollover, the temperature in the relatively cool lower layer increased by $350\text{ °C} \pm 50\text{ °C}$ ($600\text{ °F} \pm 90\text{ °F}$).

Figure 18 shows the temperature data measured by the thermocouple array located in the corner of the compartment. At this location, gas temperatures, with respect to time, were approximately the same as in the center of the compartment.

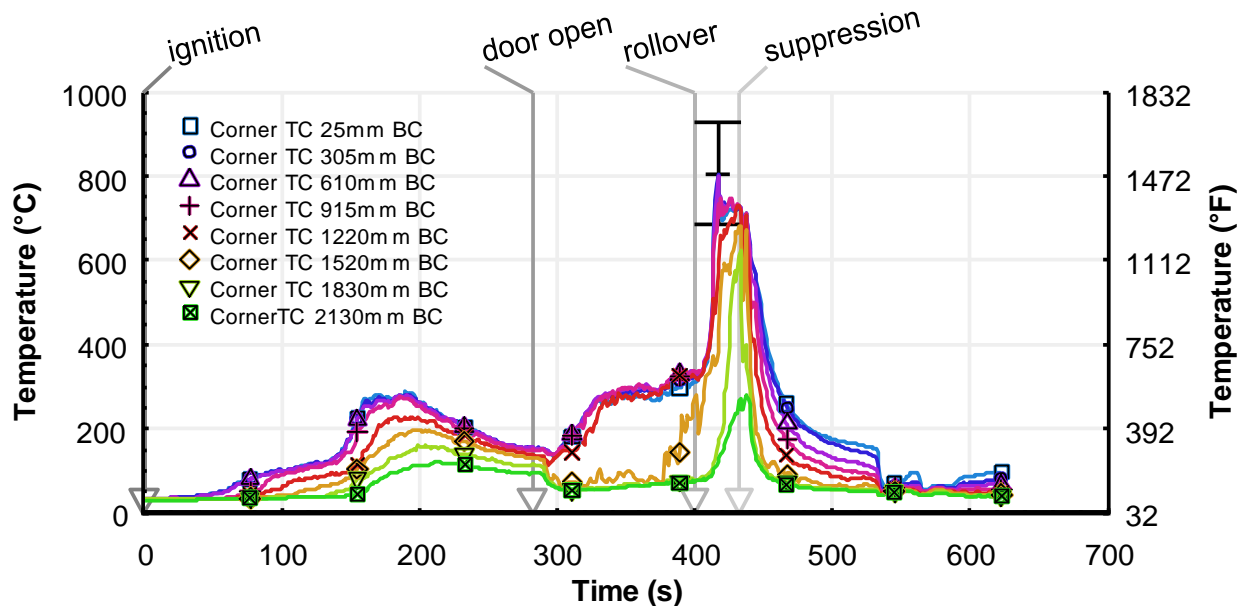


Figure 18: Floor to ceiling temperatures measured by the thermocouple array in the corner in Experiment 1

⁶ For the purposes of this paper, “rollover” is a general term that is used to define a combination of complex processes that occur during the period of fire growth. During rollover, flames spread from the first item(s) ignited to fuels in the upper gas layer. Rollover requires that the unburned products of combustion in the upper layer be in adequate quantity, sufficiently heated, and turbulently mix with an adequate supply of oxygen to sustain flame spread. Rollover may cause a compartment fire to transition to flashover, because the spread of flames through the upper gas layer exponentially increases convective and radiative heat flux in a compartment. Rollover is often, but not always visibly observable.

Figure 19 shows the total heat flux measured at the floor level in the center of the compartment and on the wall between the two FFPE samples. Heat flux began to rise above ambient level approximately 160 s after ignition. After 160 s, heat flux at the floor level remained constant, below approximately 5 kW/m^2 , until rollover. The heat flux was higher at the wall location, measuring approximately 5 kW/m^2 until rollover. The heat flux rose rapidly in both locations and both locations measured a peak heat flux of approximately 50 kW/m^2 . Suppression occurred before flashover. As a result, both measurements appear to be similar in magnitude in the few seconds before suppression. If the experiment continued without suppression, the flux would have continued to increase rapidly until a post-flashover condition. The total flux at the sample gauge was dominated by convective flux (see Figure 22), because it was located within the sooty hot gas layer. The total heat flux measured at the floor was dominated by radiative flux. The heat flux gauge on the floor was convectively cooled from incoming air, but subject to radiative flux from the large surface area of burning gasses at the hot gas layer interface. Figure 20 is a still photograph captured from the experiment video that shows these conditions inside the compartment just prior to suppression⁷. The locations of the total heat flux gauges are indicated.

Heat flux rapidly dropped to near ambient levels after suppression, but remained slightly elevated. This was likely the result of hot compartment surfaces continuing to radiate to the flux gauges.

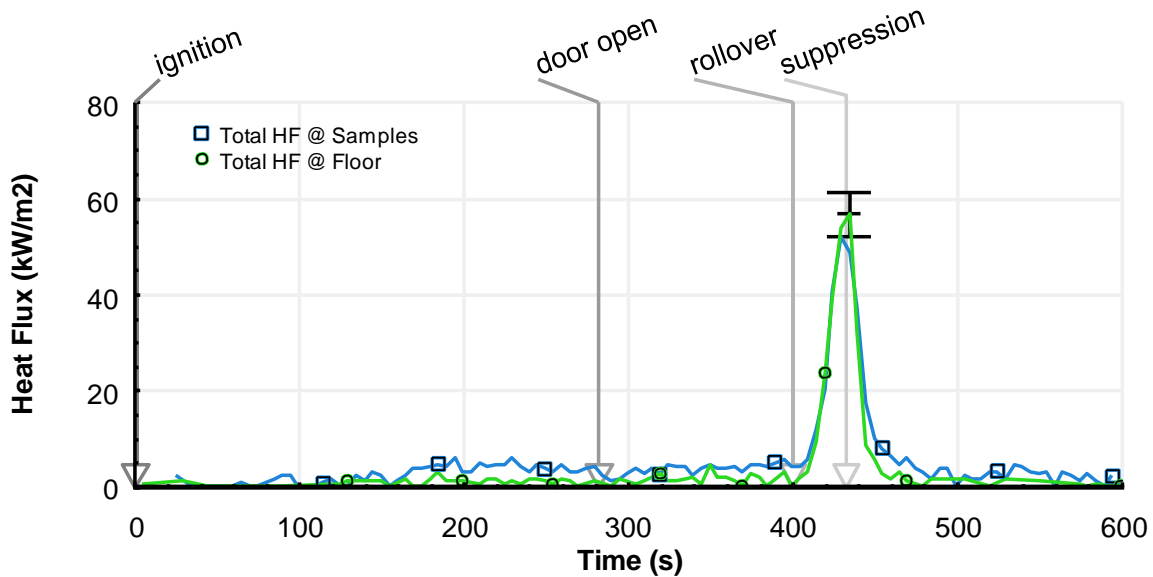


Figure 19: Total heat flux measured by the heat flux gauge next to the PE samples and by the gauge in the center of the compartment on the floor in Experiment 1

⁷ These conditions are also shown well in the second experiment. In the case of the second experiment, flames extend from the compartment window, demonstrating the underventilated conditions of the compartment.

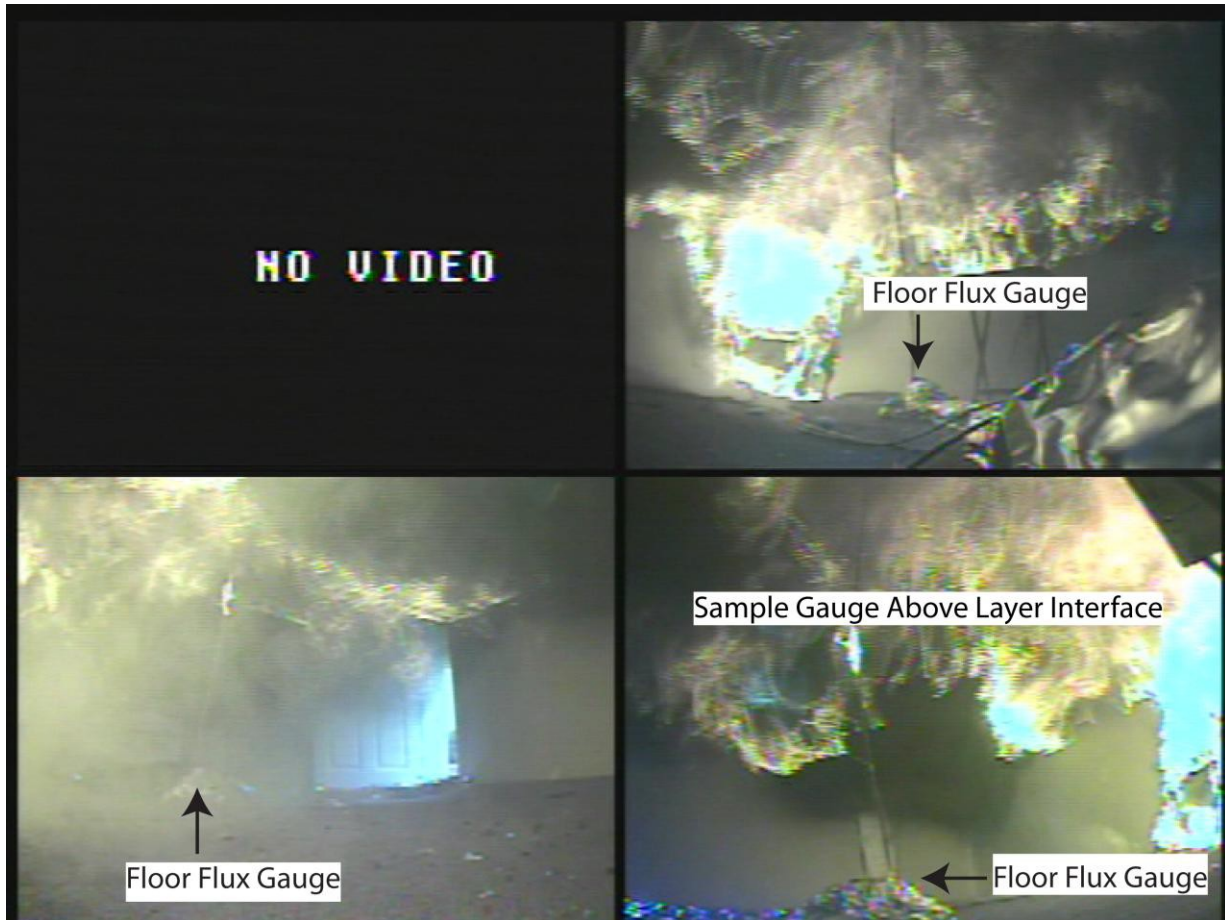


Figure 20: Video frame capture of compartment conditions immediately prior to suppression, with locations of total HF gauges indicated

Figure 21 shows the velocities of the gasses measured by the bi-directional probes positioned in the centerline of the doorway. After the door was opened, smoke vented out the doorway above 1.0 m (3.4 ft), while outside air entered and flowed into the doorway below 1.03 m (3.38 ft). As the oxygen from the fresh air mixed in the compartment, the fire on the upholstered chair resumed burning and spreading. As a result, the velocity of the gasses venting out the top of the door steadily increased until rollover. After rollover, the neutral plane lowered due to the greater volume of hot gasses venting from the compartment, descending to an elevation below 1.03 m (3.38 ft). After suppression, the elevation of the neutral plane increased and the velocity of the gasses venting out the door decreased. Gasses continued to vent from the top of the doorway until the end of the experiment.

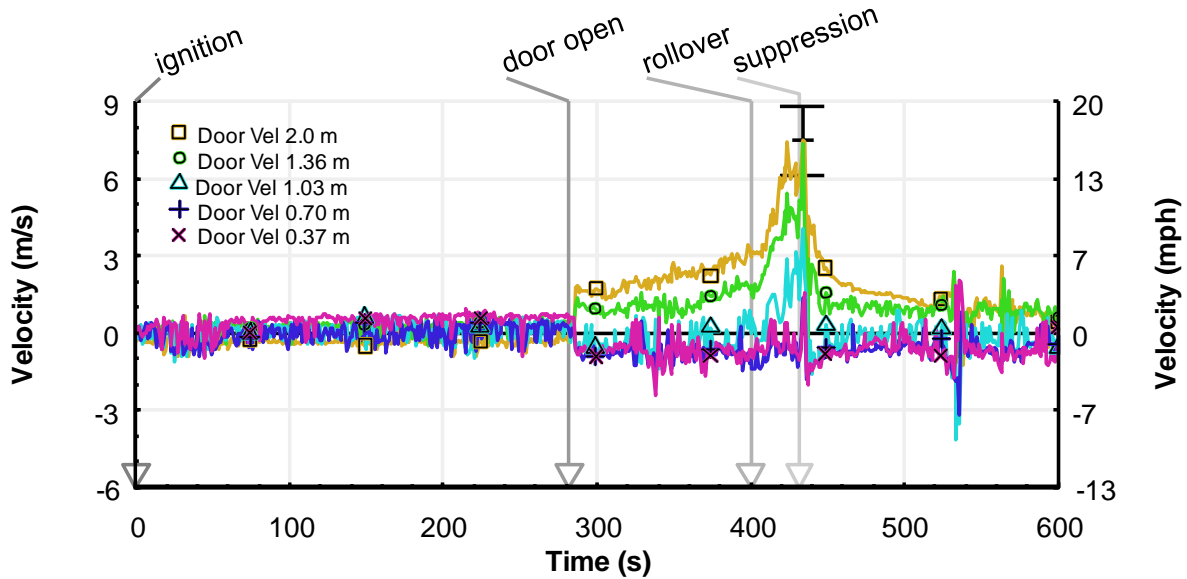


Figure 21: Velocity of gasses measured along the centerline of the front door in Experiment 1

4.1.2 Thermal Measurements from Sample Location

To provide insight into the modes of heat transfer that delivered thermal energy to the samples, Figure 22 shows a comparison of the total heat flux with radiative heat flux measured at the sample location during experiment 1. From ignition until rollover, the flux measured by the radiometer remained below approximately 5 kW/m^2 . After rollover began, the hot upper layer descended below the elevation of the FFPE samples. The radiant flux increased from approximately 3 kW/m^2 to a peak of approximately 10 kW/m^2 . Total heat flux increased from approximately 5 kW/m^2 to 55 kW/m^2 . Given these measurements, the dominant mode of heat transfer to the samples was convection. Convection accounted for more than half of the total heat flux at the sample location prior to rollover. After rollover began, convection accounted for the majority of the total heat flux. At the peak total heat flux of 55 kW/m^2 , approximately 45 kW/m^2 or 80% was convective flux, and 10 kW/m^2 was radiative.

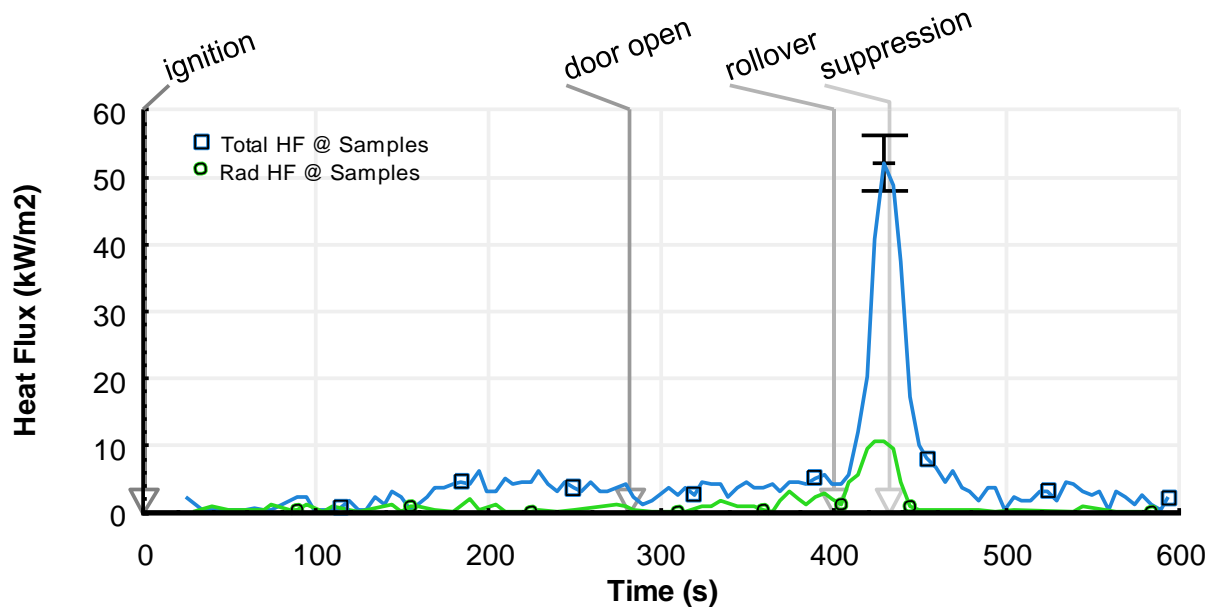


Figure 22: Total heat flux compared with radiative heat flux measured in experiment 1

Figure 23 shows a comparison of the outer shell temperature that resulted from the thermal exposure, with the temperature measured on the interior liner for the unmodified FFPE sample. As rollover occurred at approximately 400 s, the hot upper layer descended below the elevation of the FFPE samples (shown by the thermocouple at elevation 1.52 m below the ceiling in Figure 18, and visually in Figure 20) and bathed the samples in hot gasses. The total heat flux (Figure 22) incident on the samples rapidly increased, which caused a rapid increase in the outer shell temperature. The temperature of the outer shell peaked at $550 \text{ }^\circ\text{C} \pm 80 \text{ }^\circ\text{C}$ ($1020 \text{ }^\circ\text{F} \pm 150 \text{ }^\circ\text{F}$), approximately 430 s from ignition. As rollover began, the interior liner temperature was $80 \text{ }^\circ\text{C} \pm 10 \text{ }^\circ\text{C}$ ($180 \text{ }^\circ\text{F} \pm 20 \text{ }^\circ\text{F}$) and the interior liner temperature began to rise immediately. The peak in interior liner temperature of $240 \text{ }^\circ\text{C} \pm 40 \text{ }^\circ\text{C}$ ($480 \text{ }^\circ\text{F} \pm 70 \text{ }^\circ\text{F}$) occurred approximately 50 s later. The peak interior liner temperature occurred after suppression, as the thermal energy delivered to the outer shell continued to conduct through the FFPE materials.

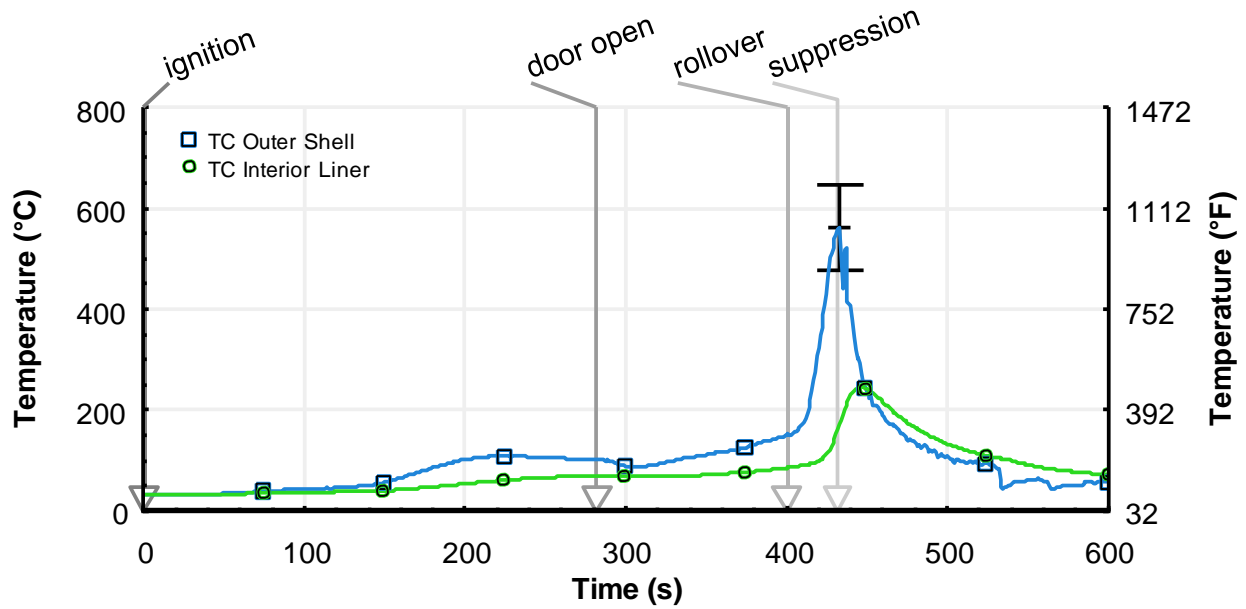


Figure 23: Comparison of the temperatures measured on the surface of the outer shell and the surface of the interior liner for the unmodified FFPE sample, Experiment 1.

Figure 24 shows the temperatures measured on the surface of the outer shell and the temperature measured on the surface of the interior liner, for the FFPE sample with PCM. The temperature measured on the outer shell was similar to the outer shell temperature for the unmodified FFPE sample for the duration of the experiment. The close proximity of the samples resulted in similar thermal exposures. However, temperature rise in the interior liner for the FFPE with PCM was delayed until approximately 20 s after rollover began. The interior liner temperature increased from approximately 50 °C to 80 °C (120 °F to 180 °F), 50 s after rollover began. As with the unmodified FFPE sample, the peak interior liner temperature was measured after suppression.

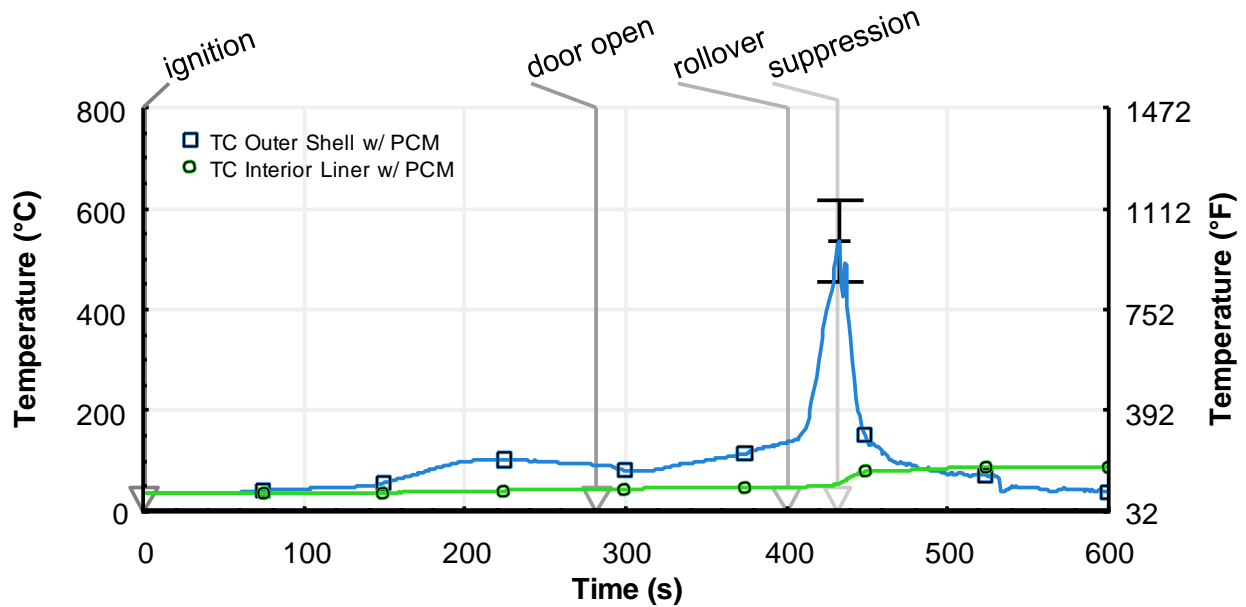


Figure 24: Temperatures measured on the surface of the outer shell and interior liner for the PE with PCM in Experiment 1

Figure 25 shows the total heat flux measured behind the unmodified FFPE sample compared with the FFPE sample with PCM. Before rollover, the total heat flux measured behind both samples remained below 1.0 kW/m^2 . As rollover began, the total flux measured behind the unmodified FFPE immediately rose, from $1.0 \text{ kW/m}^2 \pm 0.1 \text{ kW/m}^2$ to a peak value of $8 \text{ kW/m}^2 \pm 0.6 \text{ kW/m}^2$ approximately 50 s later. In the same period, the total heat flux behind the FFPE with PCM rose from below 1 kW/m^2 to a peak of $2 \text{ kW/m}^2 \pm 0.2 \text{ kW/m}^2$. For both samples, peak fluxes occurred after suppression. This demonstrates the continued transfer of thermal energy through the FFPE, even after the total incident heat flux at the sample location was reduced.

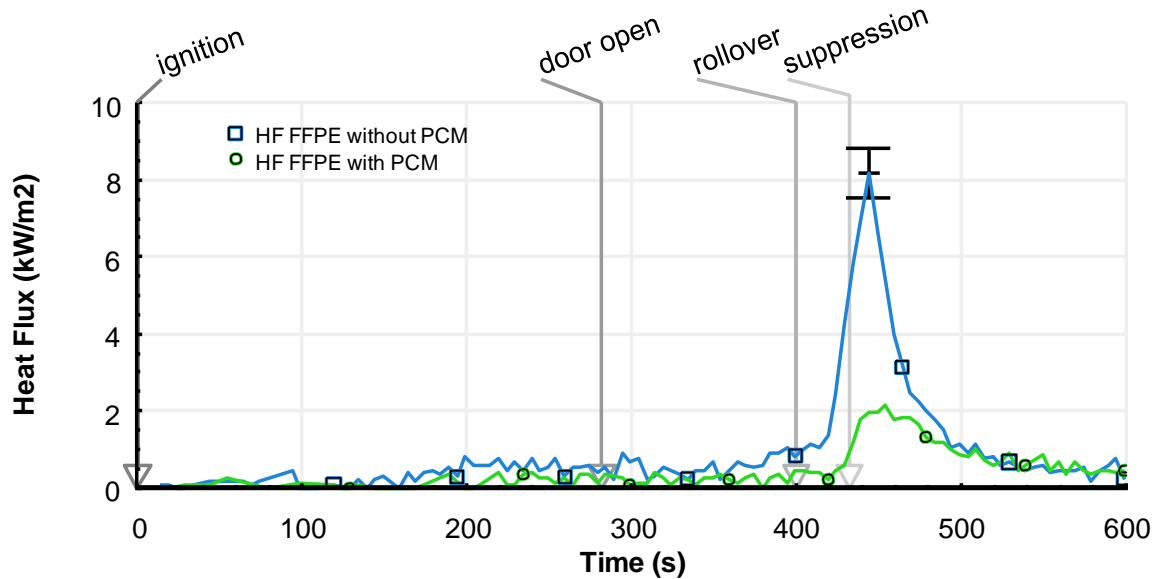


Figure 25: Total heat flux measured behind the unmodified FFPE and the FFPE with PCM in Experiment 1

Figure 26 shows both FFPE samples after the experiment. The interior liner layer in FFPE discolors when thermally degraded. The unmodified FFPE sample (left) shows more discoloration than the FFPE sample with PCM (right), indicating hotter interior liner temperatures across the unmodified FFPE sample during the experiment. Areas of discoloration are evident primarily around the plate thermometers.



Figure 26: View of the interior liner for the unmodified FFPE assembly (left) and the FFPE assembly with PCM added (right) after Experiment 1. Areas of discoloration highlighted.

4.1.3 Heat Flux Measured with Plate Thermometer

The plate thermometer was included in these experiments to examine its performance in a full-scale compartment fire test, as compared to the water-cooled S-B gauge. Figure 27 shows a comparison of the total heat fluxes measured by the S-B gauge and the total heat flux calculation based on the temperature measurement from the plate thermometer. Both measurement devices responded to the initial increase in heat flux from fire growth on the chair, at approximately 150 s. The plate thermometer was less sensitive to the low fluxes than the S-B gauge. Until rollover, the S-B gauge measured $5 \text{ kW/m}^2 \pm 0.4 \text{ kW/m}^2$, whereas the plate thermometer measures approximately half of that quantity. Once rollover started, the two devices measured approximately the same flux, responded at nearly the same rate to the rapid increase in flux, and measured approximately the same peak total heat flux of approximately 55 kW/m^2 . When suppression occurred, the two devices respond differently. The plate thermometer heat flux calculation resulted in negative heat flux after suppression. Decreasing temperatures causes the third term in the numerator of Eq. 1, which dominates the equation, to be negative⁸. However, both of the devices responded immediately to the rapid decrease in heat flux.

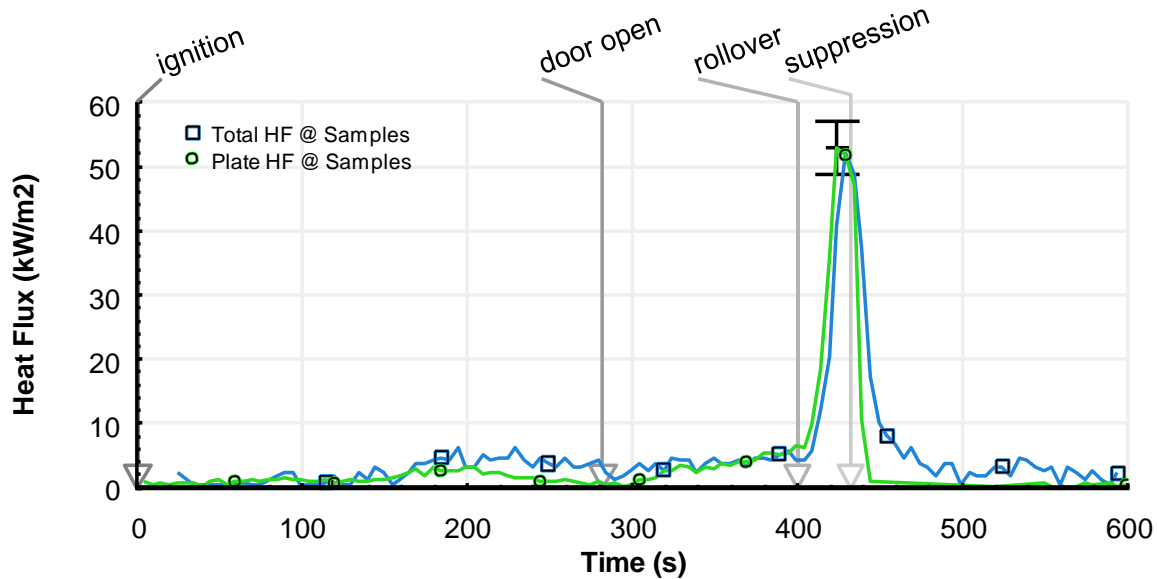


Figure 27: Comparison of the total heat flux measured by a S-B heat flux gauge and the total heat flux calculated from a plate thermocouple measurement in Experiment 1.

⁸ For Figure 27, negative fluxes calculated from plate thermometer measurements were set equal to zero.

4.2 Experiment 2: Open Door

The objective of this experiment was to evaluate the thermal hazard developed by a fire in a compartment with the door and bottom section of window open from the time of ignition. The effect of the additional ventilation from the start of the experiment was that rollover occurred in about half the time, at approximately 190 s. Flashover occurred at approximately 210 s. As in the first experiment, the interior upper pane of window glass failed after flame impingement at approximately 205 s. The remainder of the glass in the upper pane failed at approximately 245 s. The fire was suppressed at approximately 270 s by fire fighters with a 5 cm (1 ¾ in) diameter hose line.

4.2.1 Thermal Conditions inside the Compartment

Figure 28 and Figure 29 show the time history of the temperatures measured by the thermocouple array located in the center and in the corner of the compartment. Both graphs show the steady development of a hot gas layer and rollover at approximately 190 s, leading to flashover at approximately 220 s. After flashover, the thermal conditions had transitioned from a hot layer, above a cold layer, to a single well-mixed zone with temperatures effectively equal at all elevations, measuring approximately 800 °C (1472 °F) from floor to ceiling. These conditions existed until a team of fire fighters suppressed the fire at approximately 270 s.

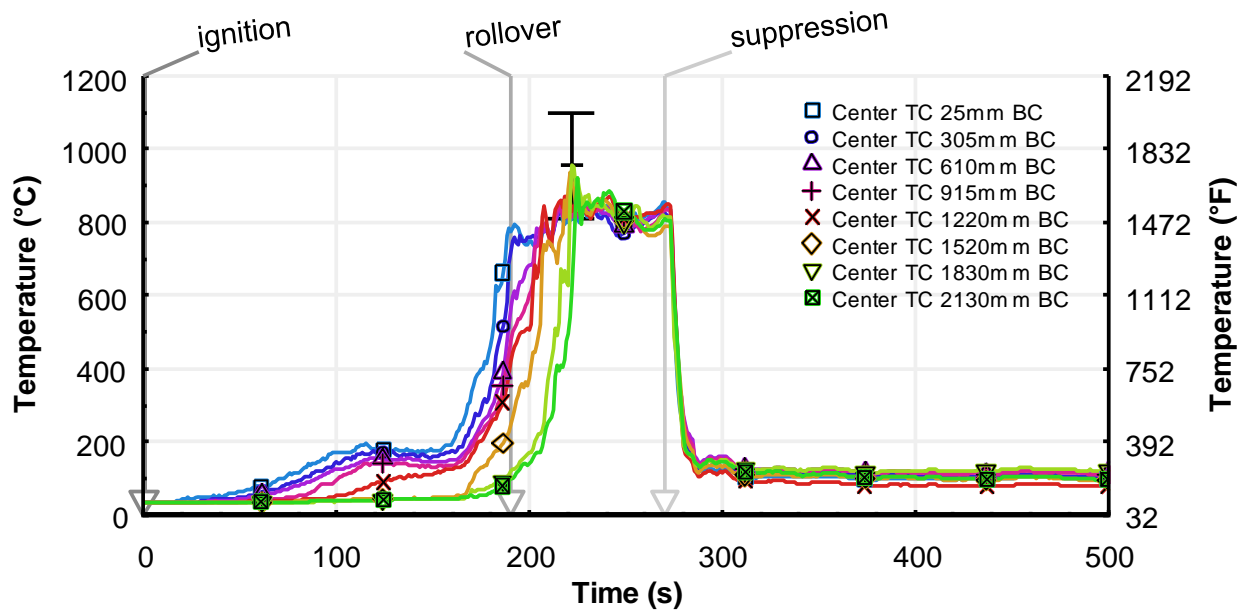


Figure 28: Floor to ceiling temperatures measured by the thermocouple array in the center of the compartment in Experiment 2

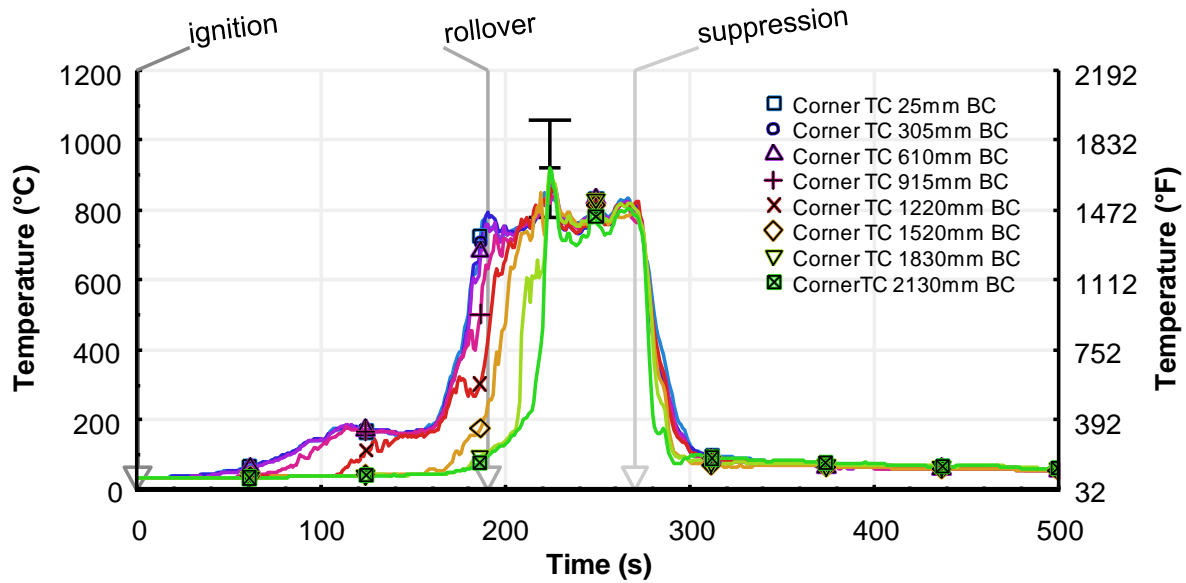


Figure 29: Floor to ceiling temperatures measured by the thermocouple array in the corner in Experiment 2

Figure 30 displays the total heat flux measured by the heat flux gauge mounted between the FFPE samples and the heat flux gauge in the center of the floor. Heat flux remained below 5 kW/m^2 in both locations until rollover occurred. A peak heat flux of approximately $70 \text{ kW/m}^2 \pm 6 \text{ kW/m}^2$ was measured between the samples at approximately 220 s. Based on the video, this peak corresponds to the time flames were burning at the interface of the hot layer, immediately in front of the gauge. A peak heat flux of approximately $95 \text{ kW/m}^2 \pm 8 \text{ kW/m}^2$ was measured at the floor at approximately 240 s. Based upon the video, the heat flux gauge completely was enveloped by flames at 240 s. Comparison of the measurements demonstrates that as the oxygen in the compartment was consumed, flaming combustion moved from the area of ignition to the areas where sufficient oxygen was available. In other words, the heat flux decreased in the area by the samples, and was consistently high in the area by the flux gauge in the center of the compartment, where flaming combustion continued.

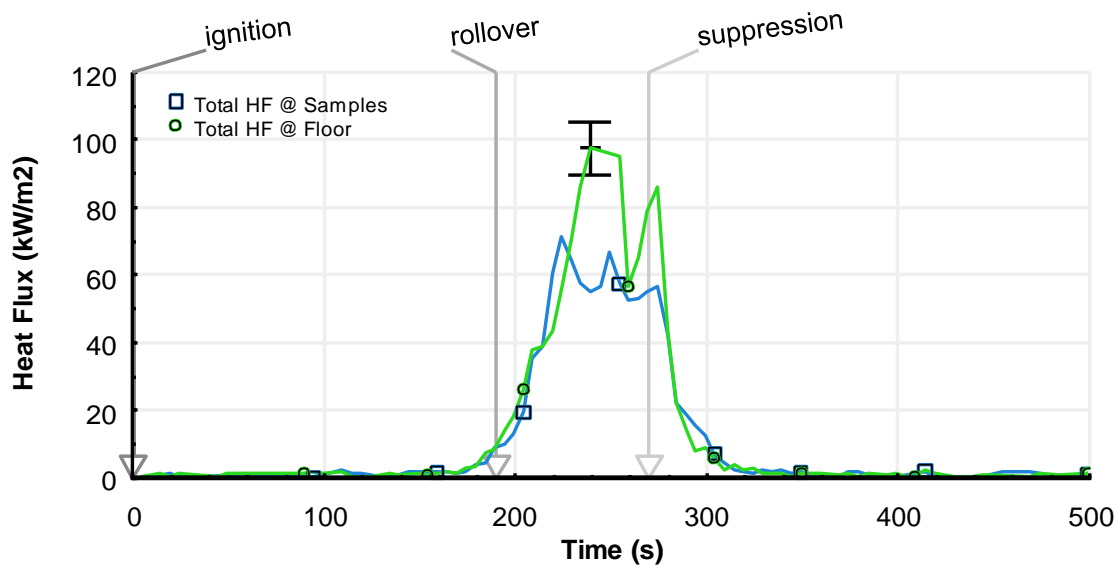


Figure 30: Total heat flux measured by the heat flux gauge next to the PE samples and by the gauge in the center of the compartment on the floor for Experiment 2

Figure 31 and Figure 32 show the velocity measurements from the bi-directional probe arrays in the centerline of the door and window. The data ends after 250 s for each graph, because heat damaged the wiring of the pressure transducers. After 60 s, the bi-directional probe 1.7 m (5.6 ft) above the doorsill began to register flow out the top of the doorway. The velocity of the flow out the top of the doorway, and into the bottom of the doorway steadily increased to approximately 2 m/s (2.2 mph \pm 0.4 mph) until just prior to rollover. After rollover, the velocities out the top of the doorway, and into the bottom of the doorway, both rapidly increased to peak flows of approximately 7 m/s \pm 1.3 m/s (15.7 mph \pm 2.8 mph). After approximately 190 s, the flow out the doorway increased and the neutral plane height dropped as low as 1.03 m (3.38 ft).

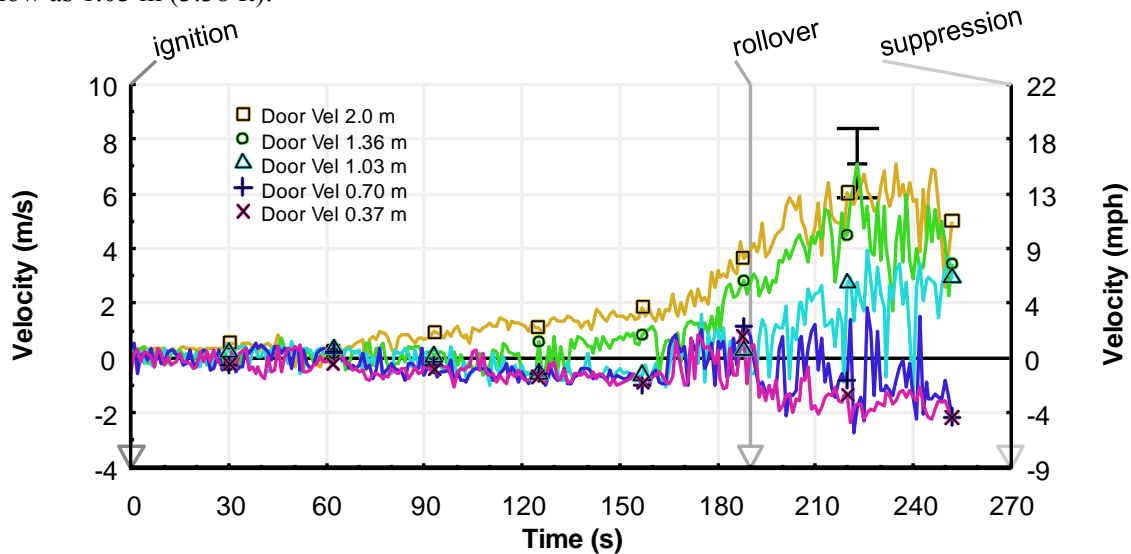


Figure 31: Velocity of gasses measured along the vertical centerline of the door in Experiment 2

After approximately 70 s, steady flow developed out of the bottom pane of the window. This flow increased until approximately 165 s, and reversed temporarily, for approximately 20 s. Based on the video, the flow reversal was due to a change in wind direction. Once rollover occurred, the pressure generated by the fire was great enough to overcome the wind, outflow resumed, and increased until a peak velocity of 8 m/s \pm 1.4 m/s. After approximately 245 s, the remaining glass broke out of the upper windowpane and allowed hot gasses to flow out.

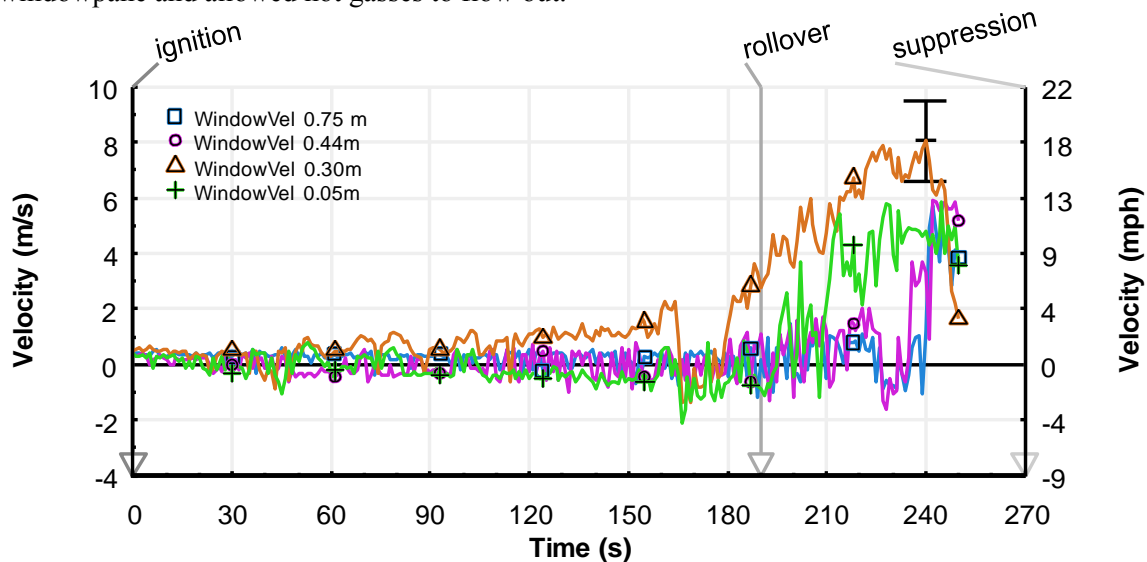


Figure 32: Velocity of gasses measured along the vertical centerline of the window in Experiment 2

4.2.2 Thermal Measurements from Sample Location

Figure 33 compares the total heat flux with radiative heat flux measured at the sample location during Experiment 2. From ignition until rollover, the radiative and total heat fluxes remained below 5 kW/m^2 . After rollover began, the total heat flux increased to a peak of $74 \text{ kW/m}^2 \pm 6 \text{ kW/m}^2$ within approximately 30 s. The peak radiative heat flux measurement occurred simultaneously, and was $30 \text{ kW/m}^2 \pm 2.5 \text{ kW/m}^2$. The radiative flux accounted for approximately 40% of the peak total heat flux. After the peak in total heat flux, the radiative flux at the sample location decreased, which caused the total heat flux to decrease. As was mentioned in the discussion of Figure 30, the compartment was under ventilated and unable to support combustion near the samples. Burning occurred where oxygen was sufficient to support combustion, due to air entrainment through the doorway. However, more burning occurred than in Experiment 1. Having been allowed to transition to flashover, the peaks of the heat flux time histories are higher and wider than in Experiment 1.

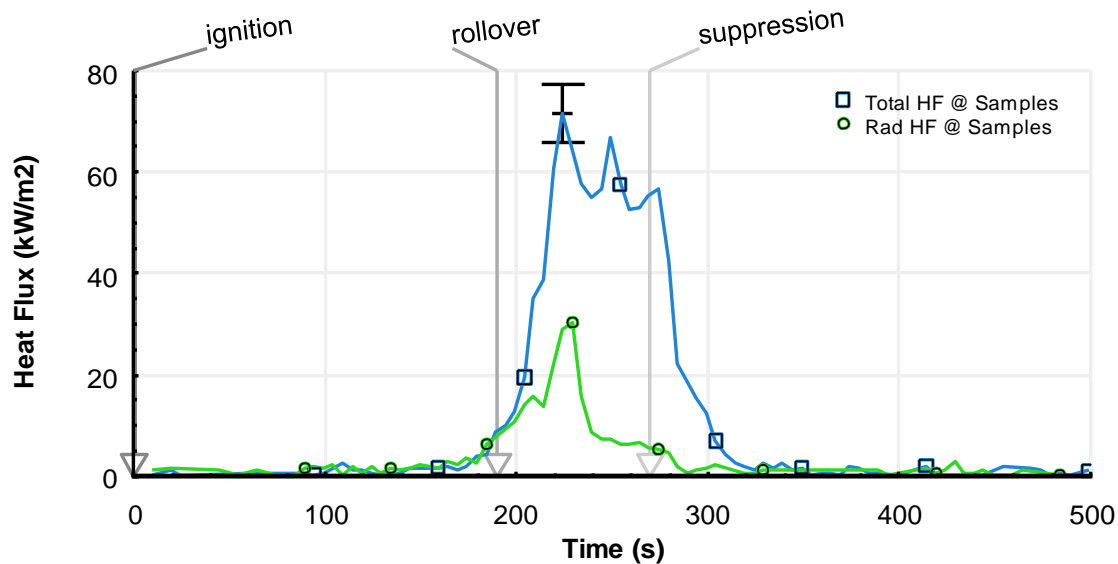


Figure 33: Comparison of the total heat flux measured by a S-B heat flux gauge and the radiative heat flux measurement in Experiment 2

Figure 34 compares the outer shell temperature, with the temperature measured on the interior liner for the unmodified FFPE sample. Until approximately 160 s, the outer shell temperature rose only approximately $10 \text{ }^\circ\text{C}$ ($18 \text{ }^\circ\text{F}$). After 160 s, the hot gas layer descended to the elevation of the thermocouple on the outer shell. This increased the total heat flux incident on the shell, and the outer shell temperature began to increase exponentially. Within 20 s (at 190 s), rollover began. In the 30 s proceeding rollover flashover occurred, and the outer shell temperature increased by approximately $650 \text{ }^\circ\text{C}$ ($1170 \text{ }^\circ\text{F}$).

The temperature increase of the interior liner was negligible prior to rollover. The interior liner temperature increased exponentially after rollover began. The interior liner temperature increased by approximately $60 \text{ }^\circ\text{C}$ ($110 \text{ }^\circ\text{F}$) before flashover, near 220 s. The interior liner temperature increased by $420 \text{ }^\circ\text{C} \pm 65 \text{ }^\circ\text{C}$ ($760 \text{ }^\circ\text{F} \pm 110 \text{ }^\circ\text{F}$) within 10 s once flashover occurred. It is likely that the FFPE burned through as flashover occurred, based upon the rate of interior liner temperature change, and the thermal damage shown in Figure 37.

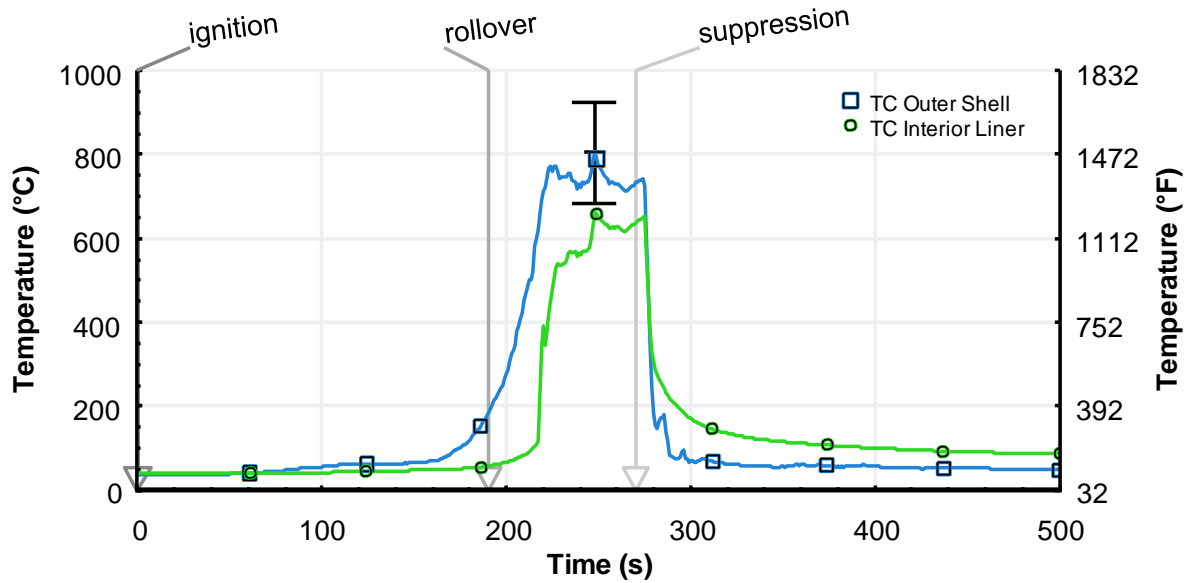


Figure 34: Comparison of the temperature measure on the surface of the outer shell with the temperature measured on the surface of the interior liner of the unmodified FFPE in Experiment 2

Figure 35 shows the outer shell temperature, with the temperature measured on the interior liner for the FFPE sample with PCM. The time history of the outer shell temperature closely resembles the time history of the outer shell temperature for the unmodified FFPE sample, because the proximity of the two samples resulted in similar thermal exposures. As with the unmodified FFPE sample, the interior liner temperature change was negligible prior to rollover. After rollover began, the added layer of PCM absorbed thermal energy passing through the FFPE and prevented the exponential rate of temperature increase observed in the unmodified FFPE sample; the interior liner temperature rose by approximately 5 °C before flashover. However, once flashover occurred at approximately 220 s, the resulting interior liner temperature behavior was the same as with the unmodified FFPE sample; the interior liner temperature increased by $410\text{ °C} \pm 60\text{ °C}$ ($740\text{ °F} \pm 110\text{ °F}$) within 10 s.

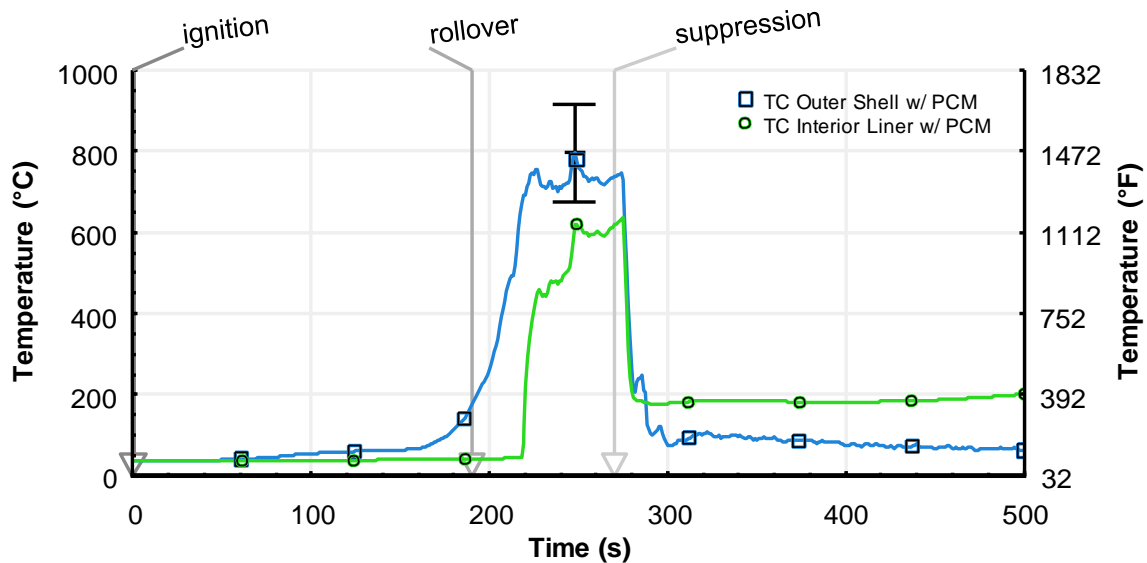


Figure 35: Temperatures measured on the surface of the outer shell and interior liner for the PE with PCM in Experiment 2

Figure 36 compares the interior liner temperatures for the unmodified FFPE sample and the FFPE sample with PCM to provide additional clarity regarding the difference in thermal measurements at the interior liner. Primarily, Figure 36 is provided to show the delay in interior liner temperature rise between the unmodified and PCM FFPE samples, in addition to the simultaneous jump in temperature rise at approximately 220 s. After suppression, the temperature of the interior liner for the unmodified FFPE may be lower for two reasons. First, the mechanical damage to the unmodified FFPE may have allowed suppression water into the FFPE, cooling the thermocouple inside the assembly. Second, the additional mass of the PCM in the modified FFPE sample may have retained thermal energy, keeping the thermocouple at an elevated temperature.

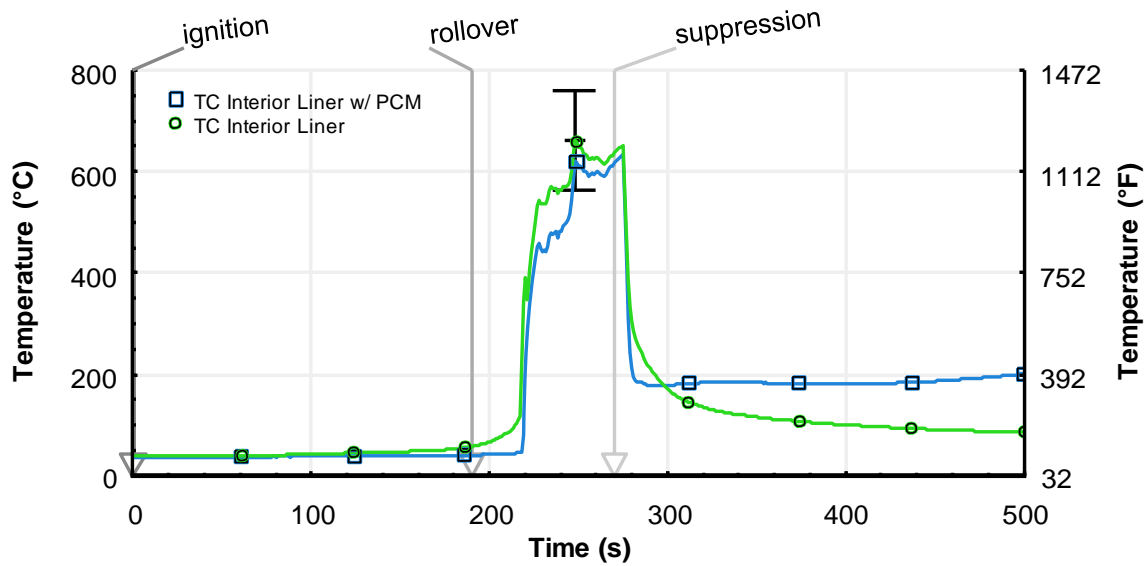


Figure 36: Temperature measured behind the unmodified FFPE and the FFPE with PCM in Experiment 2

Figure 37 shows the interior liner of both samples after experiment 2. The unmodified FFPE sample (right in photo) shows discoloring due to thermal degradation for the entire area exposed to the compartment; the area that was beneath the frame is undamaged. The greatest amount of thermal damage, where the FFPE burned completely through, occurred where the plate thermometer was located in the bottom right corner. In the plate thermometer location, the additional thermal insulation used as part of the plate thermometer construction resulted in higher local temperatures. The FFPE sample with PCM (left in photo) shows less overall damage than the unmodified FFPE sample. The perimeter of the sample frame is clear through discoloration of the interior liner, and some of interior liner shows charring. All the areas where the stitching compressed the FFPE assembly show discoloration.



Figure 37: View of the interior liner for the FFPE with PCM (left) and the unmodified FFPE (right) after Experiment 2

4.2.3 Heat Flux Measured with Plate Thermometer

Figure 38 shows a comparison of the total heat fluxes measured by the S-B gauge and the total heat flux calculation based on the temperature measurement from the plate thermometer. The plate thermometer demonstrated an increase in heat flux first, approximately 10 s before the S-B gauge. This reflects the difference in the design of each device and how each device responds to thermal flux. Part of the design of the S-B gauge involves water-cooling, and the plate thermometer has a comparatively large surface area. Additionally, the plate thermometer was located above the S-B gauge. The peak heat flux measured by the plate thermometer was $95 \text{ kW/m}^2 \pm 10 \text{ kW/m}^2$, at approximately 220 s. The peak flux measured by the S-B gauge was $70 \text{ kW/m}^2 \pm 6 \text{ kW/m}^2$, at approximately 210 s. As in experiment one, the plate thermometer measurements resulted in the calculation of negative heat flux when suppression occurred.

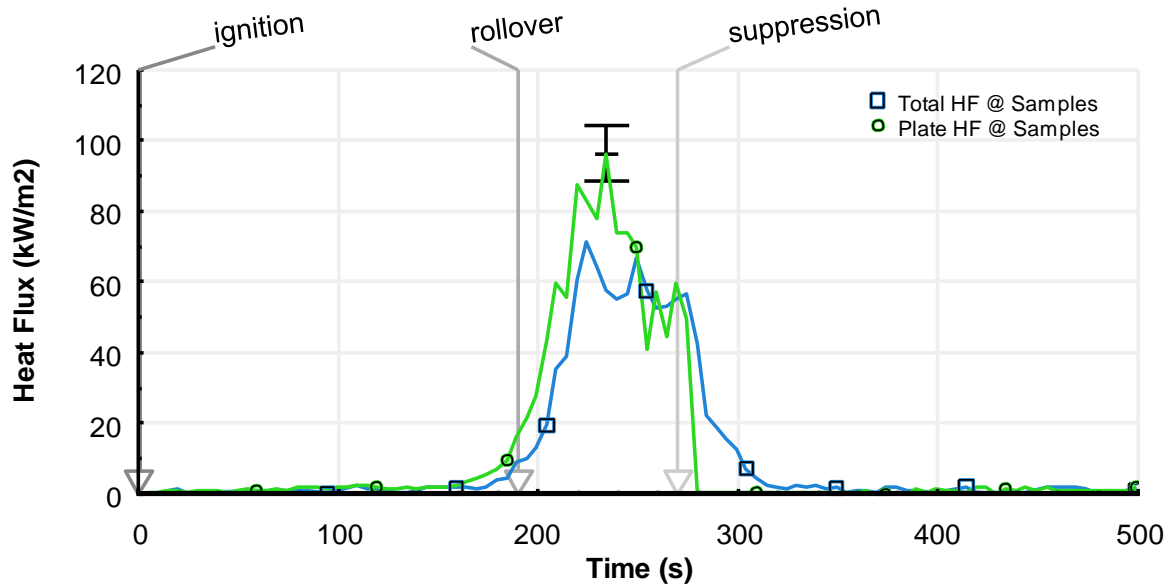


Figure 38: Comparison of the total heat flux measured by a S-B heat flux gauge and the total heat flux calculated from a plate thermocouple measurement in Experiment 2

5. Discussion

The following sections discuss the observations made from the two experiments conducted with regard to the four objectives of this report:

- Compare the thermal behavior of an unmodified FFPE sample with a sample of FFPE with PCM, exposed to a realistic interior fire fighting thermal environment
- Quantify thermal energy transfer through the unmodified FFPE sample and the FFPE sample with a layer of PCM added,
- Examine the impact of ventilation on thermal conditions inside the compartment.
- Explore plate thermometers as a simple, economical means to expand upon heat flux measurement capabilities in field experiments.

5.1 Impact of Phase Change Material

In the first experiment, the addition of a layer of PCM to a FFPE sample reduced the amount of thermal energy transferred to the interior liner material. The peak heat flux measured at the surface of the interior liner was reduced by approximately 6 kW/m^2 . The peak interior liner temperature was reduced by approximately $150 \text{ }^\circ\text{C}$. Additionally, thermal energy transfer was delayed by the PCM in the FFPE assembly; the interior liner temperature did not rise until after suppression. This may be the combined effect of the additional thermal mass of the PCM, and the energy absorbed by the phase change. For the unmodified FFPE assembly, interior liner temperature rise began approximately 30 s earlier, corresponding to the onset of rollover.

A burn injury would likely have occurred behind the unmodified FFPE sample. The peak temperature of the interior liner reached approximately $240 \text{ }^\circ\text{C}$. Even with a presumed additional layer of clothing (e.g., uniform, t-shirt and a presumptive air gap), the interior liner temperature is well above the maximum burn injury temperature assigned shown in the ASTM C 1055 burn injury prediction curve (Figure 1). Realistically, if the interior liner temperature were as hot as $240 \text{ }^\circ\text{C}$, the user would likely be burned while removing the FFPE. In the same experiment, it is less certain whether a burn injury would have occurred behind the FFPE sample with PCM; the peak interior liner temperature was approximately $90 \text{ }^\circ\text{C}$. Assuming the reduction in temperature due to additional user clothing and the relatively low thermal inertia of the FFPE materials, it is possible that a user could remove the modified FFPE assembly without incurring a burn injury. In the first experiment, outer shell temperature was not affected by the addition of PCM.

In the second experiment, the time histories of the interior liner temperature for the FFPE samples differed in only one aspect; the interior liner temperature of the unmodified FFPE sample began to rise at the onset of rollover, whereas the interior liner temperature for the FFPE sample with PCM remained at ambient until flashover. Once flashover occurred, the interior liner temperatures simultaneously increased to over $400 \text{ }^\circ\text{C}$ within seconds. This was likely due to the mechanical failure of the outer shell as a barrier against convection. For both FFPE assemblies, severe burn injuries would be certain. Figure 39 shows the thermal damage to the samples..



Figure 39: Thermal/mechanical damage to exterior of FFPE sample with PCM (left) and unmodified FFPE (right) after experiment two.

5.2 Impact of Ventilation

In the first experiment, the compartment was not provided with any means of ventilation (door closed, window closed). This resulted in fire growth until the partially burned products of combustion formed a hot layer at the ceiling that gradually descended to the elevation where the fire was located, on the seat cushion of the chair. Based on visual observations, vitiation of the flames reduced the burning rate of the chair, and the hot gas layer descended to the floor. Based on thermocouple array measurements, the gas in the compartment was effectively a single layer. The fire would potentially have self-extinguished if left unventilated. After the front door was opened, a two-zone condition was restored and the fire resumed growth. The compartment began to transition to flashover within approximately 120 s.

In the second experiment, the additional ventilation available from the time of ignition allowed the fire to grow unimpeded to a post-flashover condition. With the door and window open, a two-layer condition was maintained until flashover. With a compartment of this size, and the door and window open, the single upholstered chair provided a heat release rate large enough to enable flashover.

During the growth of the initial fire, it is possible that flow through the off-center door imposed a counter-clockwise flow within the compartment. The samples were positioned in the least direct path of fresh airflow from the door, they were located in the most oxygen-depleted region of the room. Video from the experiments shows flaming combustion at the hot gas layer interface below the samples and between the samples and the door. These conditions are shown for Experiment 1 in Figure 40 and Figure 41. Additionally, flames extended from the window and door due to the oxygen-depleted (fuel-rich) conditions in the hot gas layer.



Figure 40: Samples in oxygen-deficient hot layer, above flames, in Experiment 1



Figure 41: Samples in oxygen-deficient hot layer, above flames, in Experiment 2



Figure 42: Flames extend from the window and door due to oxygen-depleted (fuel-rich) conditions in the hot gas layer

5.3 Plate Thermometer Heat Flux Measurement

In the first experiment, the plate thermometer did not appear to be as sensitive as the S-B gauge to fluxes below 5 kW/m^2 . The plate thermometer responded nearly the same as the S-B gauge above 5 kW/m^2 and up to the peak measured flux peak of approximately 55 kW/m^2 . Once suppression occurred, the plate thermometer reported negative flux values due to the calculation of the energy balance of the instrument. This appears to be inherent to the algorithm used to represent the heat flux calculation. Given the duration of the experiment, data is not available to provide insight as to how the plate thermometer would perform for continued post-flashover heat flux measurement.

In the second experiment, the plate thermometer appeared to provide the same heat flux measurement as the S-B gauge at low heat flux levels prior to rollover ($\sim 2 \text{ kW/m}^2$). As in the first experiment, the plate thermometer responded more quickly than the S-B gauge to the rapid increase in heat flux as rollover began. Once the compartment flashed over, the plate thermometer reported a heat flux measurement 25 kW/m^2 higher than the S-B gauge. The plate thermometer continually read a higher heat flux than the S-B gauge until suppression. As with experiment one, the plate thermometer calculation produced negative heat fluxes after suppression.

6. Conclusions

This report describes two experiments in which fires were ignited in furnished compartments. These experiments were conducted by NIST in cooperation with the ATF and with the support of the USFA.

The experimental conditions were documented, including a description of the compartment geometry and construction, the fuel load in the compartments, and the location of the instrumentation used to measure gas temperature, FFPE sample temperature, total and radiative heat flux to compartment surfaces, and heat flux transferred through FFPE samples. Two experiments were conducted in which samples assemblies of FFPE, one unmodified and one with a layer of PCM added, were co-located on a compartment wall. In the first experiment, the door and window to the compartment were initially closed, and the door was opened after five minutes. In the second experiment, the door and window were open throughout the duration of the test. The results from experiments comparing the unmodified FFPE and the FFPE with PCM were presented, as well as a comparison of thermal conditions related to ventilation, and a comparison of total heat flux measured by S-B and plate thermometer heat flux gauges.

6.1 Primary objectives: thermal energy transfer through and comparison of modified and unmodified FFPE samples

In both experiments, the additional layer of PCM into the FFPE sample prevented the interior liner temperature from increasing above ambient until after rollover. In the first experiment, the PCM reduced the interior liner temperature compared to the unmodified FFPE sample, but it is unclear whether the reduction in temperature would have been sufficient to prevent a burn injury. However, compartment conditions were pre-flashover in the first experiment. In the second experiment, the interior liner temperatures for both FFPE samples increased immediately and simultaneously by several hundred degrees when flashover occurred. Despite the addition of the PCM, the performance of the two samples was effectively the same. From the data presented, it is apparent that the rate that thermal energy was delivered to the FFPE exceeded the ability of the PCM to absorb thermal energy. Under these conditions the addition of PCM to the FFPE did not provide any significant thermal protective performance of the FFPE samples, even though the quantity of PCM used was equivalent in weight to 10 layers of batting material

6.2 Secondary objectives: Impact of ventilation on compartment thermal conditions and exploratory use of plate thermometer

Results from both experiments demonstrated the importance of ventilation in controlling fire growth and the thermal hazard inside a compartment fire environment. In the first experiment, the fire approached self-extinguishment after 5 minutes without ventilation. Two minutes after the door was opened, the compartment was entering a stage of flashover. In the second experiment, the fire grew to flashover within three minutes of ignition. With respect to fire fighting tactics, this demonstrates the importance of locating the fire source in a structure, and minimizing the time between ventilation and suppression (i.e., having means of suppression prepared when ventilating).

Total heat flux measurements in both experiments demonstrated that plate thermometers might be useful to provide economical measurement of total heat flux in a potentially destructive compartment fire experiment. The S-B gauges typically used in compartment fire experiments require a reliable source of water cooling, and typically cost several thousand dollars. Plate thermometers do not require water cooling and can be assembled from readily available materials which cost on the order of hundreds of dollars. In the two experiments, the plate thermometer measurements provided the best agreement with the S-B gauge measurements when the compartment was in a pre-flashover condition. In both experiments, the plate thermometer measurements resulted in negative calculated heat fluxes when rapidly cooled.

7. Future Work

Further research should be carried out with heat transfer modeling and accompanying bench-scale experimentation to advance the understanding of the effectiveness of PCM in providing additional thermal protection in FFPE. Heat transfer modeling could be used to simulate the impact of using different PCM, different placement of PCM layers within FFPE, different FFPE materials, and multiple types/placements of PCM within FFPE. Bench-scale testing could be used to validate the heat transfer model. Additionally, further research could be carried out to develop PCM with reduced mass and increased sensible/latent heat energy storage. Eventually full-scale testing should be carried out to determine the performance of new arrangements of FFPE modified with PCM under realistic fire fighting conditions.

8. Acknowledgements

The authors would like to express their appreciation to NIST Engineering Laboratory employees Kelly Opert, and Roy McLane, for providing the engineering and technical support required to set up and carry out these experiments.

NIST would like to thank Mark Teufert of the ATF, Rick Merck of the Montgomery County (MD) Fire and Rescue Service's Office of the Fire Marshal, and Mike Donahue of the United States Fire Administration at the National Fire Academy for providing the location, materials, and construction assistance needed to carry out these experiments. NIST extends gratitude to the Mt. Weather Fire Department and the Vigilant Hose Company of Emmitsburg Fire Department for providing fire suppression services.

The authors also wish to thank Jonathan Kent for the application of his programming talents which enabled improved data analysis capabilities and graph generation.

9. References

- [1] R. Fahy, "U.S. Fire Service Fatalities in Structure Fires 1977-2009," National Fire Protection Association, Quincy, MA, 2010.
- [2] M. Karter and J. Molis, "U.S. Firefighter Injuries - 2010," Quincy, MA, October 2011.
- [3] National Fire Protection Association, "NFPA 1971: Standard on Protective Ensembles for Structural Fire Fighting and Proximity Fire Fighting," Quincy, MA, 2007.
- [4] National Fire Protection Association, "NFPA 1977: Standard on Protective Clothing and Equipment for Wildland Fire Fighting," Quincy, MA, 2011.
- [5] National Fire Protection Association, "NFPA 1992: Standard on Liquid Splash-Protective Ensembles and Clothing for Hazardous Materials Emergencies," Quincy, MA, 2005.
- [6] National Fire Protection Association, "NFPA 1991: Standard on Vapor-Protective Ensembles for Hazardous Materials Emergencies," Quincy, MA, 2005.
- [7] National Fire Protection Association, "NFPA 1994: Standard on Protective Ensembles for First Responders to CBRN Terrorism Incidents," Quincy, MA, 2007.
- [8] R. Lawson and W. Twilley, "Development of a Dynamics Compression Test Apparatus for Measuring Thermal Performance of Fire Fighters' Protective Clothing," Gaithersburg, MD, April 2000.
- [9] T. Suzuki, T. Hirayama, K. Aihara and Y. Hirohata, " Experimental studies of moderate temperature burns," *Burns*, vol. 17, no. 6, pp. 443-451, 1991.
- [10] American Society for Testing and Materials, "C 1055 Standard Guide for Heated Systems Surface Conditions that Produce Contact Burn Injuries," West Conshohocken, PA, 2009.
- [11] A. R. Moritz and F. C. Henriques, "Studies of Thermal Injury Part I, The Conduction of Heat To and Through Skin and the Temperatures Attained Therein. A Theoretical and Experimental Investigation", *American Journal of Pathology*, vol. 32, pp. 531-549, 1947.
- [12] A. Moritz and F. Henriques, "Studies of Thermal Injury Part II. The Relative Importance of Time and Surface Temperature in the Causation of Cutaneous Burns," *American Journal of Pathology*, Vols. 695-720, p. 23, 1947.
- [13] A. M. Stoll and L. C. Greene, "Relationship Between Pain and Tissue Damage Due to Thermal

- Radiation," *Journal of Applied Physiology*, vol. 14, no. 3, pp. 373-382, 1959.
- [14] A. M. Stoll and M. A. Chianta, "Method and Rating System for Evaluation of Thermal Protection," *Aerospace Medicine*, November, 1969.
- [15] A. M. Stoll and M. A. Chianta, "Heat Transfer Through Fabrics as Related to Thermal Injury," *Transactions of the New York Academy of Sciences*, vol. 33, pp. 649-669, 1971.
- [16] National Fallen Firefighters Foundation, "National Fire Service Research Agenda Symposium," Emmitsburg, MD, 2005.
- [17] National Fire Protection Association, "Fire and Emergency Service Personal Protective Equipment Summary of Research Needs," Quincy, MA, May 2008.
- [18] A. Hamins, F. Amon, J. Averill, N. Bryner, D. Butry, R. Davis, R. Gann, J. Gilman, S. Manzello, A. Maranghides, N. Marsh, R. McDermott, R. Mell and J. J. Hall, "Proceedings of the 2009 Workshop on Innovative Fire Protection," Gaithersburg, MD, April 2010.
- [19] L. K. McCarthy, "The Application of Phase Change Material in Fire Fighter Protective Clothing," *Fire Technology*, p. Published Online, November 2011.
- [20] American Society of Testing and Materials, "E162: Standard Test Method for Surface Flammability of Materials Using a Radiant Heat Energy Source," West Conshohocken, PA, 2011.
- [21] R. Rossi and W. Bolli, "Phase Change Materials for Improvement of Heat Protection," *Advanced Engineering Materials*, pp. 368-373, 2005.
- [22] International Organization for Standardization, "ISO 6942: Protective clothing -- Protection against heat and fire -- Method of test: Evaluation of materials and material assemblies when exposed to a source of radiant heat," International Organization for Standardization, 2002.
- [23] International Organization for Standardization, "ISO 9151: Protective clothing against heat and flame -- Determination of heat transmission on exposure to flame," International Organization for Standardization, 1995.
- [24] Safety Components, "Glide-Specs," 22 March 2011. [Online]. Available: <http://www.safetycomponents.com/Downloads/Fire/Thermal/Glide-Specs.pdf>. [Accessed 30 December 2011].
- [25] W. L. Gore & Associates, "Gore Protective Fabrics," 10 March 2008. [Online]. Available: <http://www.goreprotectivefabrics.com/remote/Satellite?blobcol=urldata&blobheader=application%2Fpdf&blobkey=id&blobtable=MungoBlobs&blobwhere=1153996797270&ssbinary=true>. [Accessed 30 December 2011].
- [26] Safety Components, "Safety Components an ITG Company," 4 August 2010. [Online]. Available: http://www.safetycomponents.com/Downloads/Fire/Outershells/PBI_Matrix-Specs.pdf. [Accessed 30 December 2011].
- [27] DuPont, *FE eBrochure_6.29.pdf*, DuPont, 2010.
- [28] Rubitherm Technologies GmbH, "RUBITHERM® PX - Latent Heat Powder based on Paraffins," Rubitherm Technologies GmbH, Berlin, 2000.
- [29] Unifrax I LLC, "Form C-1421," Niagara Falls, New York, 12/2008.
- [30] H. Ingason and U. Wickström, "Measuring incident radiant heat flux using the plate thermometer," *Fire Safety Journal*, vol. 42, pp. 161-166, 2007.
- [31] U. Wickström, "Short communication: heat transfer by radiation and convection in fire testing," *Fire and Materials*, no. 28, pp. 411-415, 2004.
- [32] B. N. Taylor and C. E. Kuyatt, "Guidelines for Evaluating and Expressing the Uncertainty of NIST Measurement Results," Gaithersburg, MD, January 1993.
- [33] Omega Engineering, Inc., *Omega Temperature Measurement Handbook*, MMX (6th ed.), Stamford, CT: Omega Engineering, 2007.

- [34] L. Blevins, "Behavior of Bare and Aspirated Thermocouples in Compartment Fires," in *National Heat Transfer Conference, 33rd Proceedings*, Albuquerque, NM, December 2001.
- [35] W. M. Pitts, E. Braun, R. D. Peacock, H. E. Mitler, E. L. Johnsson, P. A. Reneke and L. G. Blevins, "Temperature Uncertainties for Bare-Bead and Aspirated Thermocouple Measurements in Fire Environments," in *Thermal Measurements: The Foundation of Fire Standards, ASTM STP 1427*, Dallas, TX, December 2001.
- [36] A. Robbins and P. Collier, "Heat Flux Measurements: Experiments and Modeling," BRANZ, Ltd., Judgeford, New Zealand, 2009.
- [37] Medtherm Corporation, "Medtherm Corporation Bulletin 118, "64 Series Heat Flux Transducers", " Hunstville, AL, August 2003.
- [38] W. Pitts, A. Murthy, J. de Ris, J.-R. Filtz, K. Nygard, D. Smith and I. Wetterlund, "Round robin study of total flux gauge calibration at fire laboratories," *Fire Safety Journal*, no. 41, pp. 459-475, 2006.
- [39] Setra Systems, "Very Low Pressure Transducer Data Sheet Rev. G," Boxborough, MA, January 2008.
- [40] Ohaus Corporation, Manual for SD Series Bench Scale, Pine Brook, NJ, 2000.

Appendix A: Plate Thermometer Temperature Measurements

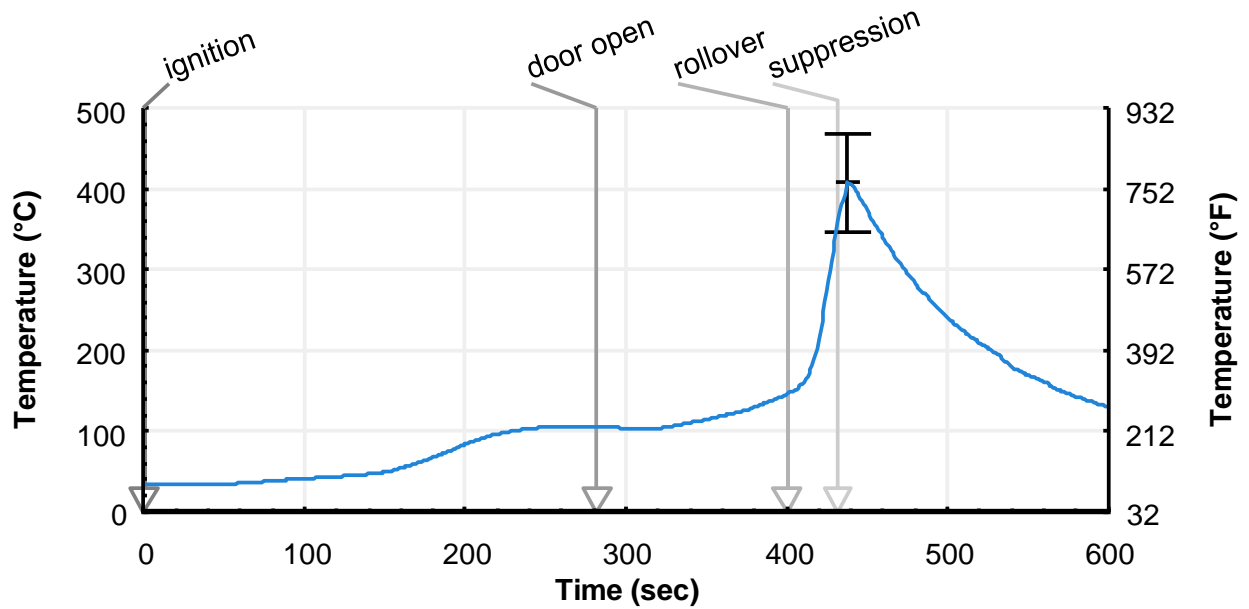


Figure 43: Plate thermometer temperature measurement from between the FFPE samples, Experiment 1

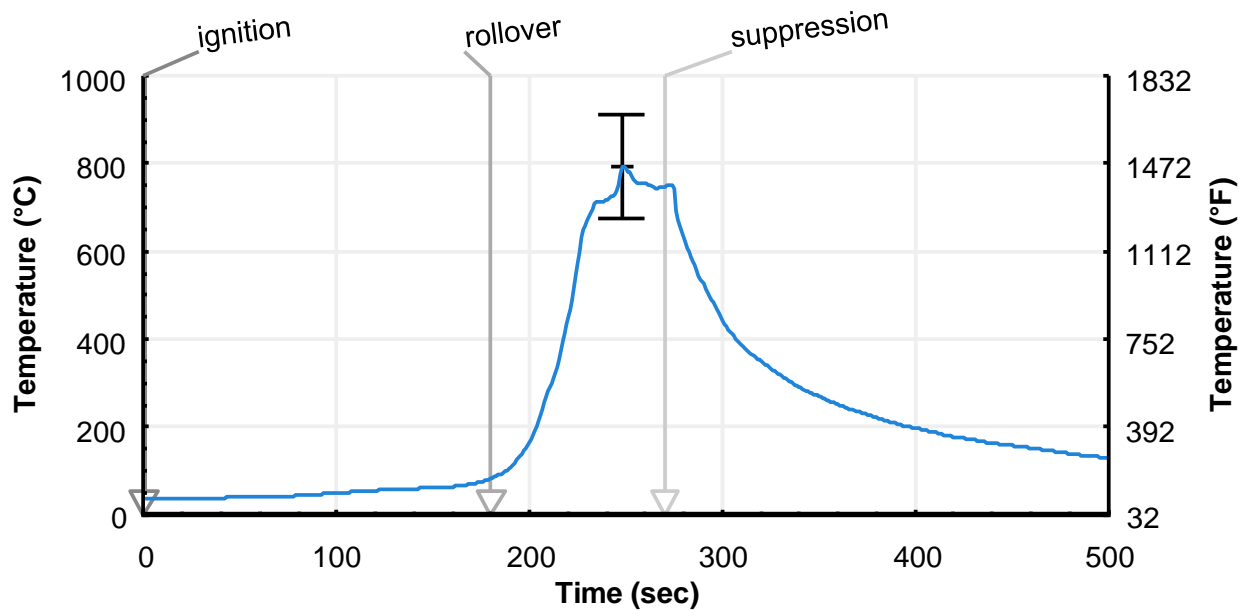


Figure 44: Plate thermometer measurement from between the FFPE samples, Experiment 2

Appendix B: Bi-Directional Probe Pressure and Temperature Measurements

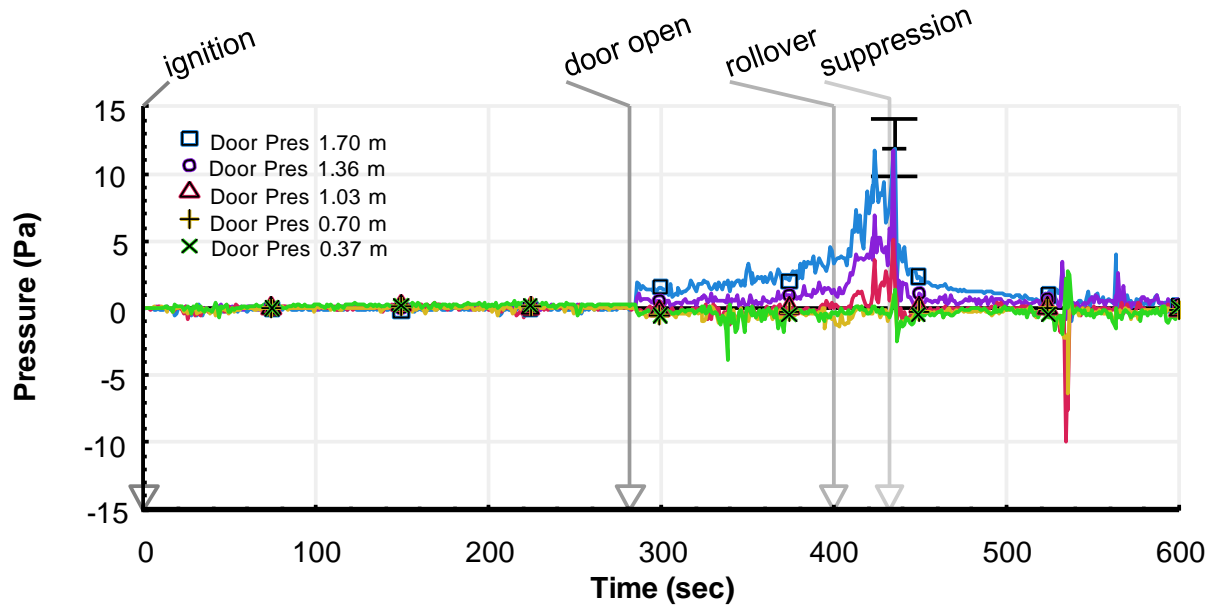


Figure 45: Bi-Directional probe pressure measurements through doorway centerline, Experiment 1

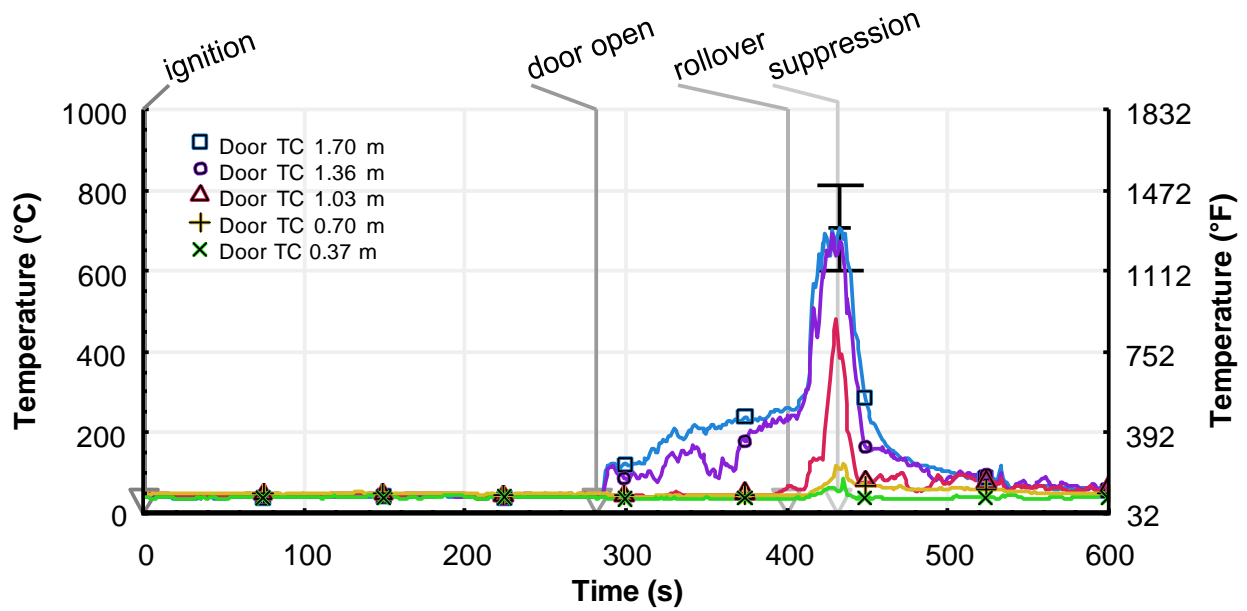


Figure 46: Temperatures measured by thermocouples located in centerline of doorway, Experiment 1

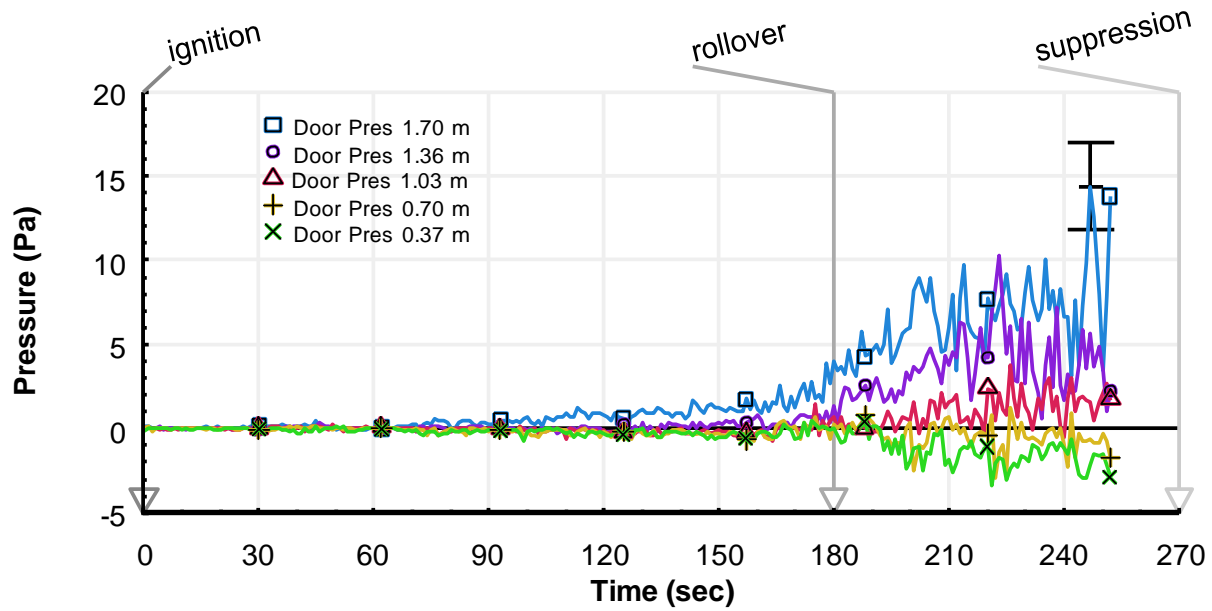


Figure 47: Bi-Directional probe pressure measurements through doorway centerline, Experiment 2

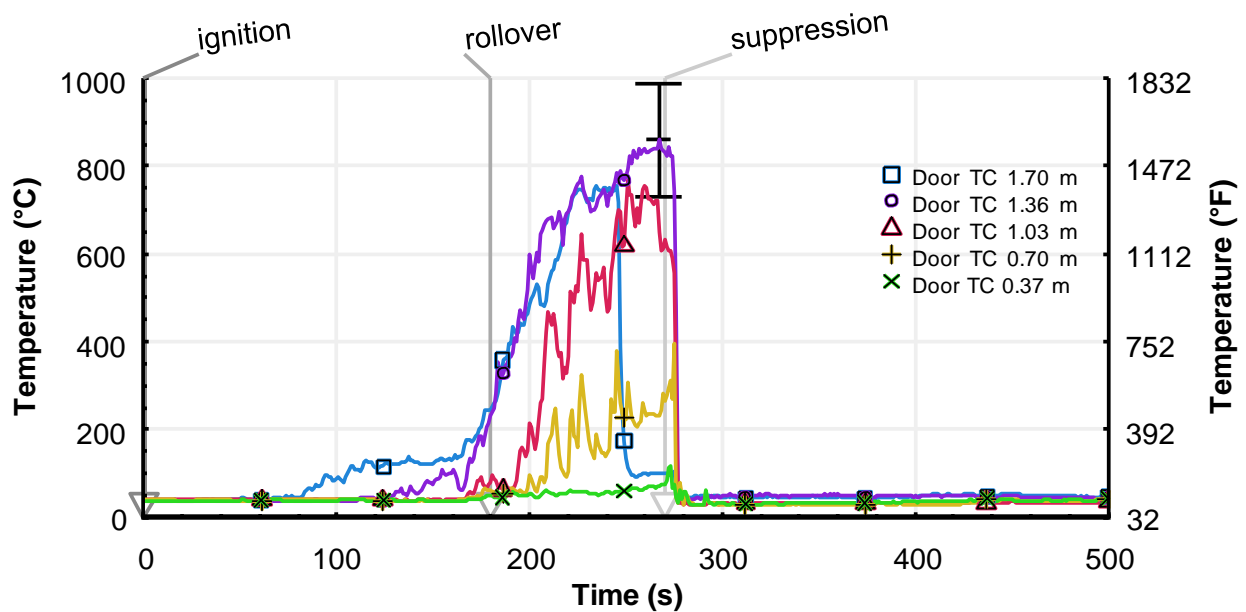


Figure 48: Temperatures measured by thermocouples located in centerline of doorway, Experiment 2

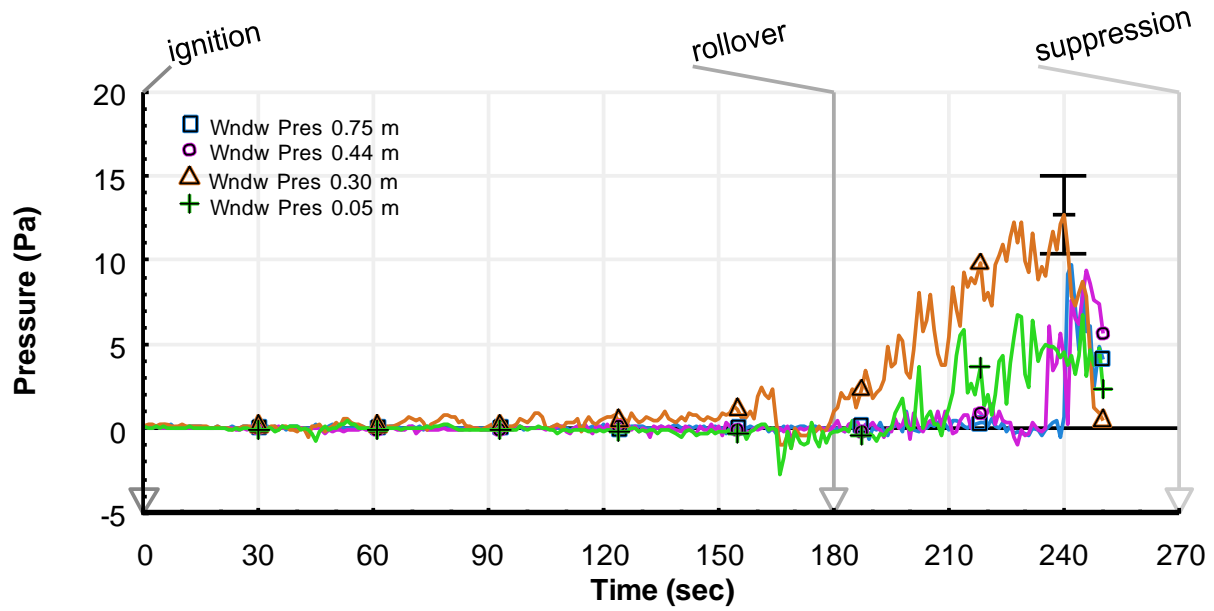


Figure 49: Bi-Directional probe pressure measurements through window centerline, Experiment 2

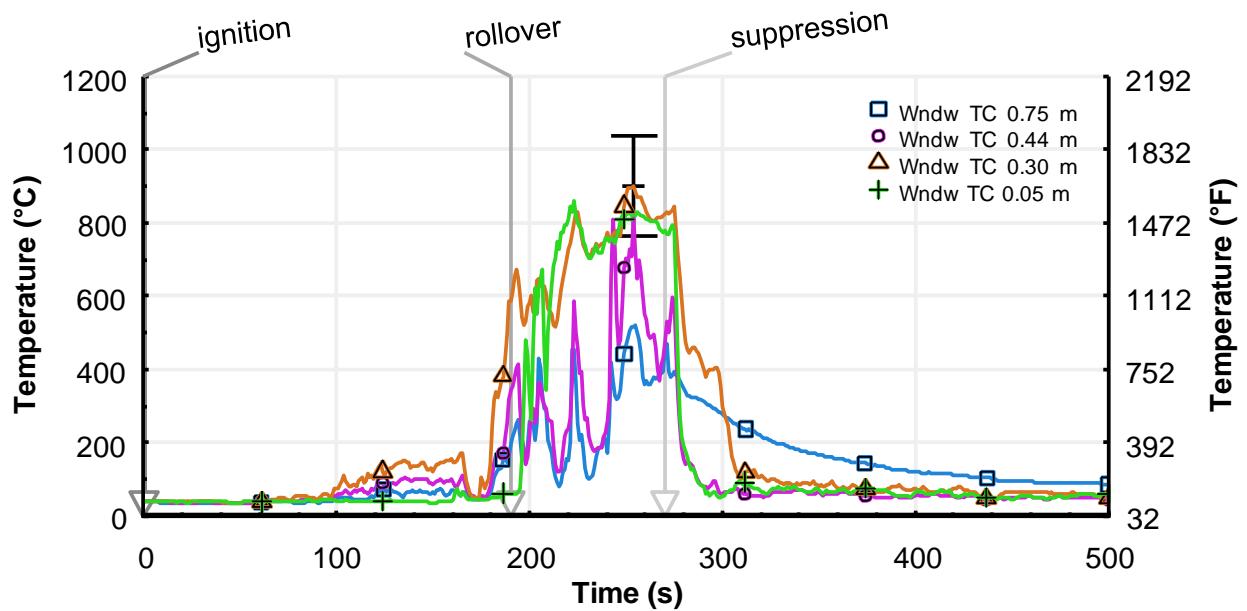


Figure 50: Temperatures measured by thermocouples located in centerline of window, Experiment 2